Biochimica et Biophysica Acta 1788 (2009) 1482–1496

Contents lists available at ScienceDirect

Biochimica et Biophysica Acta

journal homepage: www.elsevier.com/locate/bbamem

Evidence of pores and thinned lipid bilayers induced in oriented lipid membranes interacting with the antimicrobial peptides, magainin-2 and aurein-3.3

Chul Kim, Justin Spano, Eun-Kyung Park, Sungsool Wi *

Department of Chemistry, Virginia Tech, Blacksburg, VA 24061, USA

ARTICLE INFO

Article history:
Received 31 January 2009
Received in revised form 22 April 2009
Accepted 22 April 2009
Available online 3 May 2009

Keywords:
^{31}P and ^{2}H solid-state NMR
Antimicrobial peptide
Magainin-2
Aurein-3.3
Lipid bilayer
Elliptic toroidal pore
Thinned membrane bilayer
Lateral diffusion

ABSTRACT

Dynamic structures of supramolecular lipid assemblies, such as toroidal pores and thinned bilayers induced in oriented lipid membranes, which are interacting with membrane-acting antimicrobial peptides (AMPs), magainin-2 and aurein-3.3, were explored by ^{31}P and ^{2}H solid-state NMR (ssNMR) spectroscopy. Various types of phospholipid systems, such as POPC-d_{31}, POPC-d_{31}/POPG, and POPC-d_{31}/cholesterol, were investigated to understand the membrane disruption mechanisms of magainin-2 and aurein-3.3 peptides at various peptide-to-lipid (P:L) ratios. The experimental lineshapes of anisotropic ^{31}P and ^{2}H ssNMR spectra measured on these peptide–lipid systems were simulated reasonably well by assuming the presence of supramolecular lipid assemblies, such as toroidal pores and thinned bilayers, in membranes. Furthermore, the observed decrease in the anisotropic frequency span of either ^{31}P or ^{2}H ssNMR spectra of oriented lipid bilayers, particularly when anionic POPG lipids are interacting with AMPs at high P:L ratios, can directly be explained by a thinned membrane surface model with fast lateral diffusive motions of lipids. The spectral analysis protocol we developed enables extraction of the lateral diffusion coefficients of lipids distributed on the curved surfaces of pores and thinned bilayers on a few nanometers scale.

1. Introduction

Membrane-acting antimicrobial peptides (AMPs), which are produced by many tissues and cell types in a variety of invertebrate, plant and animal species, destroy the cell membranes of invaded microorganisms, such as bacteria, fungi, protozoa, and enveloped viruses as well as malignant cells and parasites [1–10]. Because D- and L-amino acid versions of antimicrobial peptides generally show little selectivity in binding, the antimicrobial action of AMPs appears to involve direct attacks on the cell membrane rather than accompanying any of the protein-based receptors and transporters on the cell surface of microbes, resulting in depolarization, permeabilization, and lysis [11–14]. On the contrary, some receptor-mediated AMP binding effects were also reported [15,16]. AMPs, which consist of 5–50 amino acid residues, can be categorized into five major classes: α-helical, defensin-like (cystein-rich), β-sheet, peptides with an unusual composition of regular amino acids, and bacterial and fungal peptides containing modified amino acids [17]. Despite their diverse types of membrane-induced secondary structures, all AMPs display a similar motif: an amphiphilic structure, with one surface highly positive (hence, hydrophilic) and the other hydrophobic.

For AMPs forming membrane-acting secondary structures upon binding to lipid membranes, two commonly reported modes are the "*S*-state", in which the peptide is bound approximately parallel to the membrane surface, and the "*I*-state", in which the peptide is inserted in the membrane approximately parallel to the membrane normal [18–21]. A surface-bound *S*-state [22] would be favorable when the peptide concentration is low because cationic AMPs can bind electrostatically to the anioinic headgroups of lipid bilayers. If the peptide concentration reaches a threshold value, a few closely placed AMP molecules may insert into bilayers after forming an intermolecular peptide bundle, leading to a transition from a *S*-state to an *I*-state. Molecules and ions can transport across the cell membranes through this pore, resulting in the lysis of a cell due to the destruction of an osmotic pressure gradient existing across the cell membranes. A transition from a *S*-state to an *I*-state has a sigmoidal peptide concentration dependence, suggesting cooperativeness in the peptide–membrane interactions [23–26]. In addition to these, though, is the "*T*-state", in which the peptide inserts into the membrane such that the helix axis is oriented approximately 120° to the membrane normal. The "*T*-state" was initially reported for PGLa [27–30], but has also been seen for MSI-103 [29] and MAP [31]. Also reported are barrel-stave model [32], peptide-induced inverted hexagonal phases [33,34], and detergent-type micelles [35] involving certain lipids and peptides.

In this study, we have investigated the membrane binding properties of a known AMP, magainin-2 [18,36], and an unknown AMP, from the aurein family, aurein-3.3 [5,9,37–39]. Both magainin-2, an α-helical structured 23-residue peptide found on the skin of the African clawed frog *Xenopus laevis*, and aurein-3.3, an unknown

* Corresponding author. Tel.: +1 540 231 3329; fax: +1 540 231 3255.
E-mail address: sungsool@vt.edu (S. Wi).

0005-2736/$ – see front matter © 2009 Elsevier B.V. All rights reserved.
doi:10.1016/j.bbamem.2009.04.017

structured 17-residue AMP present in the secretion from the granular dorsal glands of the Green and Golden Bell Frog *Litoria aurea*, possess a broad-spectrum of antimicrobial activity against various types of bacteria, virus, and fungi. Moreover, magainin-2 and aurein-3.3 receive our particular attention because they possess potential drug activities against diabetic foot ulcers and cancer cells, respectively.

Reportedly, magainin-2 forms a *S*-state at a low peptide concentration and makes a transition to an *I*-state after a critical peptide concentration in phospholipids bilayers [18,26,40–42]. The behavior of aurein-3.3 is still unknown. In this manuscript, we have investigated the membrane-disrupting characteristics of magainin-2 and aurein-3.3 in oriented phospholipid bilayers by investigating ^{31}P and ^{2}H ssNMR spectra of lipids. Various compositions of oriented lipid bilayers were studied, including zwitterionic phosphatidylcholine (PC), anionic phosphatidylglycerol (PG), and cholesterol. We have evidenced the existence of peptide-induced supramolecular lipid organizations, such as toroidal pores and thinned membrane bilayers, that are under the influence of dynamic lateral diffusions of lipids in cell membrane mimetic media, as exemplified in ^{31}P and ^{2}H ssNMR spectra. A spectral analysis protocol [43] recently developed was applied for simulating the spectral characteristics of such AMP-induced supramolecular lipid assemblies. Our lineshape analysis protocol provides a means to extract the lateral diffusion coefficients of lipids located on curved membrane surfaces, such as pores or thinned bilayers, on a few nanometers scale which may hitherto have been difficult to characterize.

2. Experimental procedures

2.1. Materials

All phospholipids were purchased from Avanti Polar Lipids (Alabaster, AL). These include 1-palmitoyl-2-oleoyl-*sn*-glycero-3-phosphotidylcholine (POPC), 1-palmitoyl-d_{31}-2-oleoyl-*sn*-glycero-3-phosphotidylcholine (POPC-d_{31}), and 1-palmitoyl-2-oleoyl-*sn*-glycero-3-phosphotidylglycerol (POPG). Antimicrobial peptides, magainin-2 (GIGKFLHSAKKFGKAFVGEIMNS; HPLC purity: 98.9%; MW: 2466.90) and aurein-3.3 (GLFDIVKKIAGHIVSSI-CONH$_2$; HPLC purity: 98.3%; MW: 1796.20), were purchased from GL Biochem (Shanghai, China) and EZBiolab Inc. (Westfield, IN), respectively, and used without further purification. Trifluoroethanol (TFE), naphthalene, chloroform and sodium phosphate dibasic were purchased from the Aldrich Chemicals (Milwaukee, WI). Thin cover-glass plates (~80 μm in thickness) cut into rectangles of 10 mm × 5 mm in width were obtained from the Marienfeld Laboratory Glassware (Bad Mergentheim, Germany).

2.2. Preparation of oriented phospholipid bilayers

A known, standard procedure [44,45] was used to prepare mechanically oriented lipid bilayers between thin cover-glass plates. Peptides and phospholipids dissolved in TFE and chloroform, respectively, were mixed to produce peptide-to-lipid (P:L) molar ratios of 0:100, 1:80, 1:50, and 1:20. The solution was air-dried and redissolved in a chloroform/TFE (2/1) solution containing a 5-fold excess amount of naphthalene. The solution was deposited onto thin cover-glass plates at a surface concentration of 0.01–0.04 mg/mm^2, air-dried, and then vacuum-dried overnight to remove residual organic solvents and naphthalene. The dried sample was directly hydrated with 2 μl of water and placed in a chamber containing a saturated solution of Na_2HPO_4, which provides about 95% relative humidity, for 2 days [46,47]. The full hydration condition of the lipids used in our study was confirmed by Yamaguchi et al. previously by FT-IR measurements: the amount of water was 50 ± 3 wt.% [48]. About 10 or 15 glass plates were stacked together, wrapped with parafilm, and sealed in a polyethylene bag to prevent dehydration during ssNMR measurements. When a fully hydrated condition was desired, an additional 2–4 μl of water was applied to the plates along the sides of the stack before wrapping [47,49].

2.3. Solid-state ^{31}P and ^{2}H NMR spectroscopy

^{31}P and ^{2}H ssNMR experiments were performed on a Bruker (Karlsruhe, Germany) Avance II 300 MHz spectrometer operating at the resonance frequencies of 300.12 MHz for ^{1}H, 121.49 MHz for ^{31}P, and 46.07 MHz for ^{2}H. A static double-resonance probe, equipping a rectangular, flat coil with inner dimension of 18 × 10 × 5 mm, was used for measuring static ^{31}P and ^{2}H ssNMR spectra of oriented phospholipid bilayers confined between thin cover-glass plates that are interacting with AMPs. The temperature of the sample compartment in the NMR probe was maintained at 20 °C by using the BCU-X temperature control unit. The ^{31}P chemical shift was referenced to 85% H_3PO_4 at 0 ppm. The pulse power calibrations of ^{31}P and ^{2}H channels were carried out by using 85% H_3PO_4 and D_2O solutions, respectively. The 90°-pulse durations of ^{31}P and ^{2}H pulses incorporated in our NMR experiments were both 5 μs. ^{31}P spectra were acquired with a single 90° pulse with a ^{1}H decoupling power of 45 kHz and a recycle delay of 2 s. The ^{2}H spectra were acquired using a quadrupolar echo sequence, 90° (or 45°)–τ_{echo}–90°–detection [50], with an echo delay time τ_{echo} = 30 μs, while incorporating a short recycle delay of 0.3 s. The spectral widths of ^{31}P and ^{2}H ssNMR spectra were 20 and 100 kHz, respectively. ^{31}P and ^{2}H spectra were typically averaged over 2048 and 12000 scans, respectively. ^{31}P 2D exchange spectra were obtained by using a conventional three pulse sequence, 90°–t_1–90°–τ_m–90°–detection (t_2) [51], with τ_m = 5–200 ms, to examine lateral diffusive motions of lipids in a slow motional regime by correlating orientation-dependent frequencies at two different measurement times, t_1 and t_2, that are separated by a mixing period τ_m.

3. Theoretical considerations

3.1. Calculation of anisotropic ^{31}P and ^{2}H NMR spectra of lipids

Anisotropic ^{31}P and ^{2}H ssNMR spectra can readily be used to characterize disordered structures of lipids in membrane bilayers [52–55]. Anisotropic ssNMR lineshapes of ^{31}P chemical shift anisotropy (CSA) and ^{2}H quadrupolar coupling (QC) interactions would reveal the angular distributions of ^{31}P and ^{2}H sites in lipids, and therefore, the orientation of lipids with respect to an applied magnetic field. When a two-tailed phospholipid in a bilayer is considered under a sufficiently hydrated condition, a fast uniaxial rotation of the lipid within a few nanoseconds around its chain axis, which is collinear to the direction of the local bilayer normal, forms a motionally averaged, axially symmetric CSA tensor of the ^{31}P nucleus in the lipid [56]. Fig. 1A explains how a rapid, uniaxial rotation of a phospholipid around its chain axis, which is collinear to the principal axis component δ_{22} of the ^{31}P's CSA, provides motionally averaged CSA tensor elements $\delta_{//}$ (= δ_{22}) and δ (= $(\delta + \delta_{33})/2$) (Fig. 1B). Thus, lipids involved in, for instance, a liposome provide a narrower ^{31}P NMR CSA powder pattern, specified by motionally averaged tensor elements, $\delta_{//}$ and δ. Lipids in a uniformly aligned bilayer would provide a single sharp peak at the $\delta_{//}$ position because lipids are aligning uniformly along a single direction that is parallel to the membrane normal direction. QC tensor parameters of deuterons located in the hydrophobic acyl chains of a perdeuterated lipid, such as POPC-d_{31}, also follow the same motional averaging mechanism as the CSA tensor parameters in the ^{31}P nucleus of the hydrophilic headgroup, resulting in motionally averaged, axially symmetric QC tensor parameters.

An observed anisotropic frequency of a site in a lipid in either a ^{31}P or ^{2}H ssNMR spectrum depends on the spatial position of the site in the applied magnetic field direction B_0. The observed anisotropic NMR frequencies of lipids distributed on a curved membrane surface can

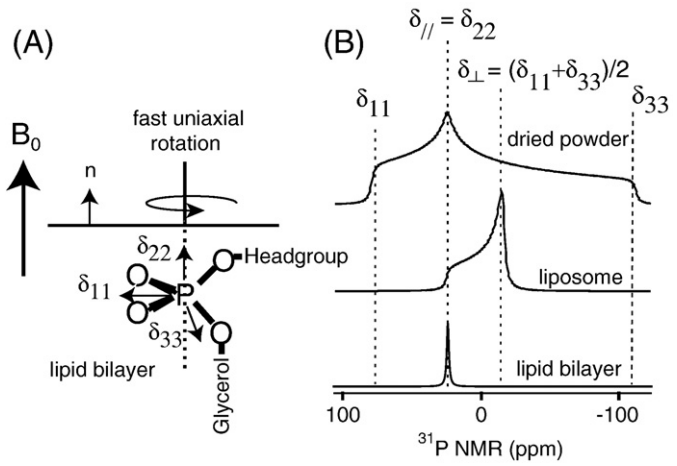

Fig. 1. (A) A fast, uniaxial rotation of a phospholipid in a lipid bilayer around its chain axis, which is collinear to the intrinsic δ_{22} component of the ^{31}P CSA of the phosphate group, makes motionally averaged, uniaxial ^{31}P CSA tensor components: $\delta_{//}=\delta_{22}$; $\delta=(\delta_{11}+\delta_{33})/2$. (B) The ^{31}P CSA powder pattern measured on dried powders (top row) decreases into a motionally averaged, narrower CSA pattern for lipids distributed on a liposome (middle row) due to the fast uniaxial rotations of lipids. When the bilayer normal n of a lipid bilayer is collinear to the applied magnetic field, B_0, phospholipids aligned in an oriented lipid bilayer provide a sharp line at the 0° position, which is identical to the $\delta_{//}$ direction (bottom row).

therefore be determined by a surface integral over an Euler angle set, $\Omega(0^\circ, \theta, \phi)$, as [43]

$$\nu_\lambda(\Omega) = \int_\Omega \nu_\lambda(0^\circ, \theta_i, \phi_i) p(\Omega) d\Omega, \tag{1}$$

where $p(\Omega)$, a probability density function that is directly proportional to an infinitesimal surface area at Ω, is called an anisotropic NMR lineshape factor. For lipids distributed on a liposome, the ssNMR lineshape factor, $p(\Omega)$, is $sin\theta$. For lipids possessing a cylindrical or planar distribution, it is 1. The ν_λ term is an anisotropic ssNMR frequency measured at the laboratory frame (rotating frame in the usual sense) provided by

$$\nu_\lambda = \frac{1}{h} R^\lambda_{2,0} T^\lambda_{2,0} \ (\lambda \text{ is CSA or QC}), \tag{2}$$

where h is the Plank constant and $R_{2,0}$ and $T_{2,0}$ are the spatial part and the spin part of NMR tensor parameters, respectively. The spin part tensors, $T_{2,0}$ terms, that commute with the dominant Zeeman Hamiltonian are $\sqrt{2/3}I_z$ for ^{31}P CSA and $\left(3I_z^2-2\right)/\sqrt{6}$ for ^{2}H QC interactions, respectively. The spatial tensors, $R^\lambda_{2,0}$ terms, defined at the laboratory frame can be related to the same tensors defined in the motionally averaged PAS frame by coordinate transformations via a common reference frame, a frame defined by the glass plate normal direction [43,47].

3.2. Anisotropic ^{31}P and ^{2}H ssNMR spectral lineshapes of lipids on a thinned bilayer

According to the so-called "carpet" model [57], cationic AMPs would bind preferentially to the headgroups of phospholipids before inserting into membrane bilayers, resulting in thinned membrane bilayers particularly when peptide concentration is low [20,58]. This surface-bound mode, known as a *S*-state, would produce a curved, thinned dimple in a membrane bilayer. If lipids distributed on a thinned surface of a membrane bilayer make fast lateral diffusions, the anisotropic frequency dispersion in either the ^{31}P or ^{2}H spectrum would produce a motionally averaged sharp line(s) at the center-of-mass position of the anisotropic linewidth, resulting in a decrease in the apparent frequency span in the NMR spectrum [43].

To simulate the spectral features of a membrane thinning effect, we approximated the thinned portion in a lipid bilayer to a dimple produced by the rotation of a period of the sinusoidal cosine function, which is defined on the x–z plane, around the z-axis by ϕ, as demonstrated in Fig. 2A. A portion of a peptide-bound thinned bilayer provides a curved membrane surface whose bilayer normal direction deviates from the applied magnetic field B_0. A fast uniaxial rotation of a lipid along its chain axis makes a lipid align orthogonal to the tangential line drawn on the thinned dimple where a lipid is positioning. A thinned membrane surface thus obtained would therefore result in the increase of anisotropies in ^{31}P and ^{2}H spectra. A NMR lineshape factor governed by this geometry is provided as [43]

$$\frac{a}{\pi}\sec\theta \sin^{-1}\left[\frac{a}{\pi d}\tan\theta\right], \tag{3}$$

where d and a are the depth and the radius of a dimple, respectively, and θ is an angle between the alignment axis of a lipid, which is perpendicular to the tangential line drawn on the curved spot, and the mechanical alignment direction z-axis. The relative sizes of a and d are arbitrary, but it has been reported that the thinning depth d on a cell surface due to AMP binding is in the 1–2 Å range [59]. However, on the oriented lipid bilayers interacting with an antimicrobial peptide, MSI-78, well-defined domains of thinned bilayers possessing a thin depth up to 1.1 nm have been observed in AFM studies [58]. It is convenient to use the relative ratio, d/a, for lineshape simulations. The range of angle θ varies from 0 to $\tan^{-1}(\pi d/a)$. Due to the presence of a plane of symmetry at $x=0.5a$, the range of x required for calculating θ is $0\le x\le 0.5a$. Fig. 2B demonstrates the dependence of θ on the ratio d/a. As the relative thinning depth increases, one observes an increase in the anisotropy of lipids distributed on a thinned membrane surface.

3.3. Anisotropic ^{31}P and ^{2}H ssNMR spectral lineshapes of lipids forming toroidal pores

It is widely accepted that insertions of membrane-acting AMPs into membrane bilayers induce toroidal pores in lipid membranes [45,46,60]. In our previous publication, we had introduced a general elliptic toroidal pore model to simulate the experimentally measured, anisotropic ^{31}P and ^{2}H ssNMR spectra of lipids interacting with the antimicrobial peptide protegrin-1 [43]. Anisotropic frequency distributions in either a ^{31}P or ^{2}H ssNMR spectrum of lipids located on the inner surface of an elliptic toroidal pore (Fig. 3A) can be calculated by a lineshape factor provided by

$$\frac{bd}{\sqrt{d^2\cos^2\theta + b^2\sin^2\theta}}\left(a + d - \frac{bd\sin\theta}{\sqrt{d^2\cos^2\theta + b^2\sin^2\theta}}\right), \tag{4}$$

where b, a, and d are the monolayer thickness of the lipid bilayer, the radius of a pore at its narrowest location, and the semiminor (or semimajor if $d>b$) distance of the generator ellipse defined on the x–z plane, respectively. The angle θ is considered between the z-axis defined in Fig. 3A and a line drawn from the center of the generator ellipse to the position of a lipid located on the toroidal inner surface ($0^\circ\le\theta\le 180^\circ$). For a lipid distributed on the toroidal inner surface, a fast uniaxial rotation of the lipid along its chain axis would orient the chain axis orthogonal to the tangential line drawn on the surface. Then, a modified angle (θ'), which specifies the orientation of the chain axis of a lipid with respect to the applied magnetic field direction B_0 ($z//B_0$), can be identified as

$$\theta' = \tan^{-1}\left(b^2\sin\theta / d^2\cos\theta\right). \tag{5}$$

When $d=b$, θ is equivalent to θ' and the ssNMR lineshape factor defined in Eq. (4) simplifies to $b(a+b-b\sin\theta)$, which is the case for a circular toroidal pore model reported by Ramamoorthy et al. [45].

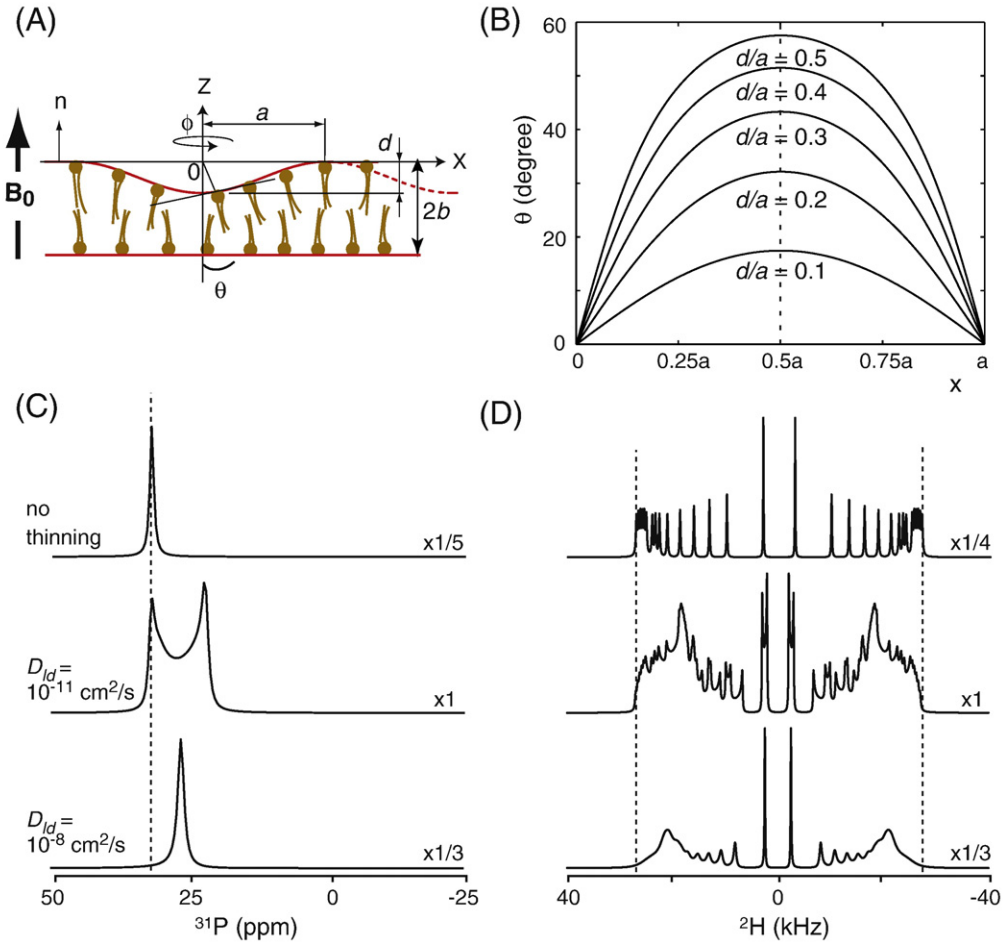

Fig. 2. (A) An AMP-induced, thinned portion of a membrane surface is approximated to a concave dimple formed by the rotation of a period of the cosine curve, defined on the *x*–*z* plane, around the *z*-axis defined at the center of the dimple, by ϕ. The depth and the radius of thus obtained dimple are defined by *d* and *a*, respectively. Lipid molecules would align orthogonal to the tangential line drawn on the curved surface of the membrane. The extent of membrane thinning is described by a d/a ratio. (B) The θ angle, which specifies the position and, therefore, the anisotropic frequency of a lipid on a thinned surface, varies in the range of 0° to $\tan^{-1}(\pi d/a)$. Ranges of θ values, depending on the d/a ratios, are shown in the figure. Expected ^{31}P (C) and ^{2}H (D) anisotropic ssNMR spectral lineshapes of POPC-d_{31} lipids distributed on a thinned membrane bilayer, specified by $b = 20$ Å, $a = 24$ Å, and $d = 4$ Å, with $D_{ld} = 10^{-11}$ cm^2/s and 10^{-8} cm^2/s. A fast lateral diffusive rate ($D_{ld} = 10^{-8}$ cm^2/s) of lipids makes a motionally averaged sharp line(s) (bottom row) at the center-of-mass position of an anisotropically broadened lineshape with a slow lateral diffusive rate ($D_{ld} = 10^{-11}$ cm^2/s) for either a ^{31}P or ^{2}H site (middle row), resulting in an apparently narrower anisotropic frequency span in the spectrum. ^{31}P and ^{2}H ssNMR spectra from a perfect bilayer are provided as a reference (top row). Tensor parameters shown in Table 1 were used in the simulations. Dashed lines are eye-guides for comparing the sizes of frequency spans.

3.4. Lateral diffusive dynamics of lipids on the curved surface of a membrane

Lateral diffusive motions of lipids occurring on the two-dimensional (2D) surface of a cell membrane would play a crucial role for the transportation of surface molecules, such as nutrients, metabolites, and drug molecules, over various regions on the cell surface. Upon binding to AMPs, lipids on cell membranes may readjust their diffusive rates due to the favorable, electrostatic peptide–lipid interactions. To better understand the dynamic nature of AMP-induced membrane assemblies, such as pores and thinned bilayers, it will be important to consider the lateral diffusive motions of lipids that may have been exemplified in the lineshapes of ^{31}P and ^{2}H ssNMR spectra.

A classical diffusion model had been incorporated previously to describe the lateral diffusions of lipids distributed on the curved surfaces of pores and thinned bilayers [43]. We assume that lipid molecules containing ^{31}P or ^{2}H sites migrate from one region to another on a curved membrane surface with a certain diffusive rate. The relative position and orientation of either a ^{31}P or ^{2}H site in the *i*th lipid on the curved surface of either a pore or thinned bilayer under the influence of an external magnetic field, B_0, can be represented by an angular point, (θ_i, ϕ_i), in a grid coordinate defined on a surface [43]. A position of a lipid, (θ_i, ϕ_i), specifies the anisotropic frequency of a site with respect to the B_0 direction. If a lateral diffusive motion is considered among a discrete set of grids, $(n\Delta\theta, m\Delta\phi)$, where *n* and *m* are integers, the orientation of either a ^{31}P or ^{2}H site in a lipid will then be encoded by an anisotropic frequency $\Omega(\theta_i, \phi_i)$. We assume that a lipid in a position, (θ_i, ϕ_i), migrates into its adjacent lattice points, $(\theta_{i\pm1}, \phi_{i\pm1})$, according to

$$(\theta_i, \phi_{i\pm1}) \xleftrightarrow{\Pi^{\phi}_{i,i\pm1}} (\theta_i, \phi_i) \xleftrightarrow{\Pi^{\theta}_{i,i\pm1}} (\theta_{i\pm1}, \phi_i), \tag{6}$$

thus, mimicking the lateral diffusion as a series of successive random walks. Because oriented lipid bilayers are confined between glass plates, we can safely ignore random translational or rotational tumbling motions of lipids or lipid assemblies [51]. The geometry dependent first-order exchange rate constants $\left(\Pi^{\theta}_{i,i\pm1}, \Pi^{\phi}_{i,i\pm1}\right)$ can be related to the diffusion coefficient D_{ld} in the standard diffusion equation defined as [54,61]:

$$\frac{d}{dt}M = D_{ld}\nabla^2 \cdot M = \Pi M, \tag{7}$$

where, M, D_{ld}, π, and ∇^2 are the column matrix that reflects the intensity of magnetization of each anisotropic frequency site in a

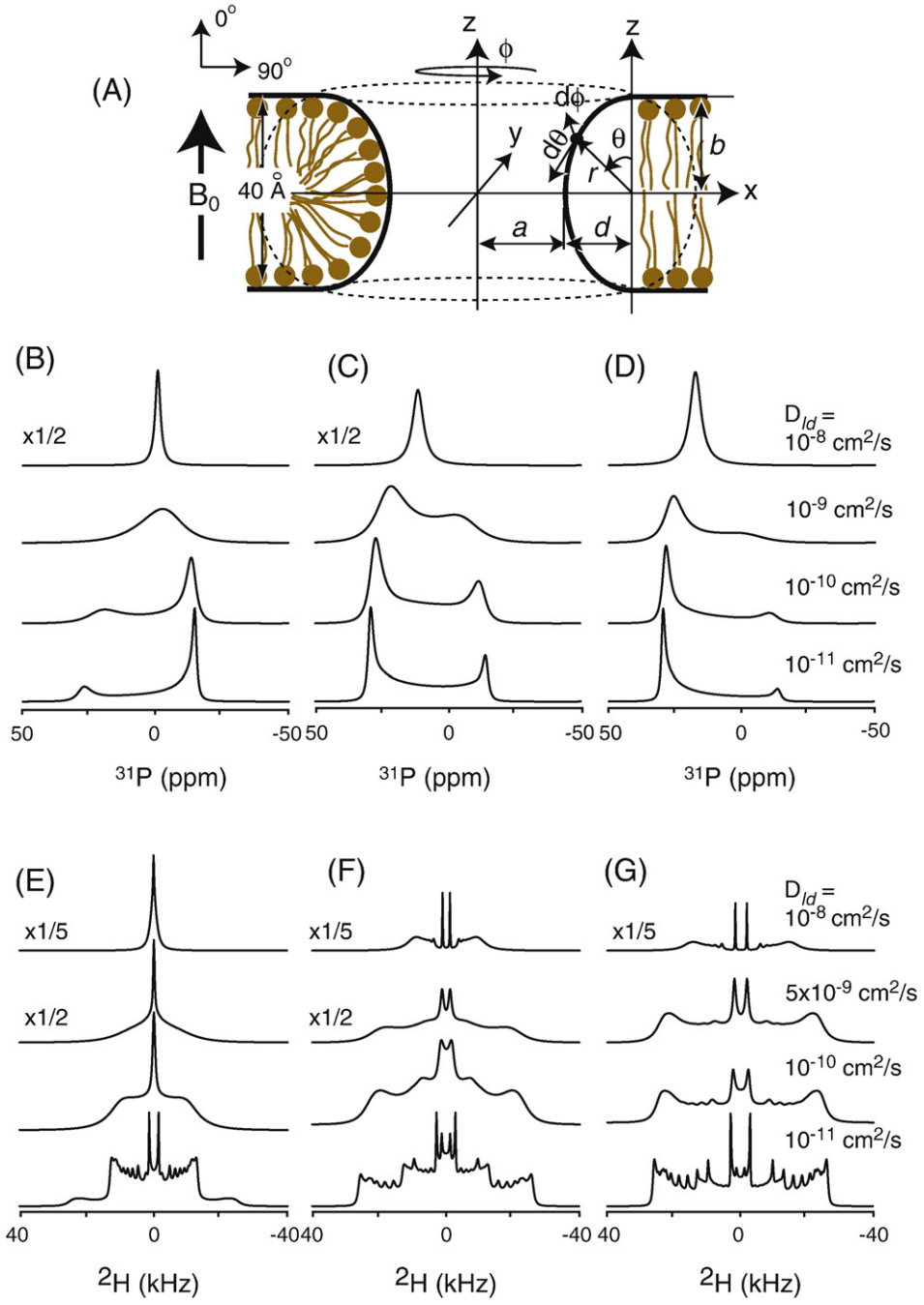

Fig. 3. An elliptic toroidal pore model introduced for describing a lipid pore formed in a flat membrane bilayer. An elliptic ring torus is characterized by the rotation of an elliptic circle, drawn on the x–z plane and described by geometric parameters r and θ, by ϕ angle about the z-axis, which is separated by the distance $a+d$ from the center of the elliptic circle. Only the inner surface of the ring torus thus obtained is considered for lipid distributions. The ranges of r, θ, and ϕ are: $d \le r \le a+d$; $0 \le \theta \le \pi$; $0 \le \phi \le 2\pi$. Parameters characterizing the overall geometrical shape of an elliptic pore are a, the radius of a pore at its narrowest location, b, the monolayer thickness of a lipid bilayers ($\approx$20 Å), and d, the elliptic semiminor (or semimajor if $d>b$) axis. The influence of a lateral diffusive rate on the anisotropic ^{31}P (B–D) and ^{2}H (E–G) ssNMR spectra of lipids located on the inner surfaces of an elliptic toroidal pore with $a=b$ and $d=0.5b$ (B, E), b (C, F), and $1.4b$ (D, G). The range of lateral diffusion coefficients considered is 10^{-8}–10^{-11} cm^2/s. Broadened lineshapes are clearly visible in the ^{31}P and ^{2}H spectra at $D_{ld} > 10^{-11}$ cm^2/s. When lipids move rapidly with $D_{ld} = 10^{-8}$ cm^2/s, a motionally averaged sharp peak is provided at the center-of-mass position of the anisotropic powder pattern of each site in either ^{31}P or ^{2}H spectra. Unlike the ^{31}P cases, a coalesced sharp peak was provided only at $d=0.5b$ in the ^{2}H spectra because the center-of-mass positions of two anisotropic powder patterns of each ^{2}H site do not coincide at other d/a ratios.

lipid, the lateral diffusion coefficient, the first-order exchange rate constant, and a coordinate-dependent *Laplacian*, respectively. A more detailed description to solve this differential equation on the curved surface of either an elliptic pore or thinned membrane bilayer is provided in the previous publication [43]. By assuming angular increments ($\Delta\theta$, $\Delta\phi$) to separate sites in the lattice, the rate constants defined along the θ and ϕ variables can be provided as

$$\Pi^{\theta}_{i,i\pm1} = \frac{D_{ld}}{h_2(\theta)h_3(\theta)}\frac{h_3(\theta \pm \Delta\theta/2)}{h_2(\theta \pm \Delta\theta/2)}\frac{1}{(\Delta\theta)^2}; \quad \Pi^{\phi}_{i,i\pm1} = \frac{D_{ld}}{h_3(\theta)^2}\frac{1}{(\Delta\phi)^2}, \tag{8}$$

where

$$h_2(\theta) = \frac{bd}{\sqrt{d^2\cos^2\theta + b^2\sin^2\theta}}; \quad h_3(\theta) = a + d - h_2(\theta)\sin\theta \qquad (9)$$

for an elliptic toroidal pore model and

$$h_2(\theta) = \sec\theta; \quad h_3(\theta) = \frac{a}{\pi}\sin^{-1}\left[\frac{a}{\pi d}\tan\theta\right] \qquad (10)$$

for a thinned membrane dimple. Then, the time evolution of anisotropic magnetizations of either ^{31}P or ^{2}H sites in lipids, distributed on a curved membrane surface, can be calculated by solving the Bloch–McConnell differential equation [62,63] that requires setting up a standard tri-diagonal NMR exchange matrix for molecular diffusions. The model suggested by Kim and Wi [43] generally considers any arbitrary orientation of the glassplate normal with respect to the applied magnetic field B_0.

Fig. 2C and D shows lineshape variations introduced in the ^{31}P (A) and ^{2}H (B) solid-state NMR spectra, respectively, of POPC-d_{31} lipids forming thinned lipid bilayers with $d/a = 0$ (top row) and $d/a = 0.167$ with $D_{ld} = 10^{-10}$ cm^2/s (middle row) and $D_{ld} = 5\times10^{-7}$ cm^2/s (bottom row), while assuming $d = 4$ Å, $z // B_0$, and $b = 20$ Å. When $d/a = 0$, the magnitude of lateral diffusion coefficient D_{ld} is irrelevant to the lineshape variations. The range of the θ angle with $d/a = 0.167$ is $0° \le \theta \le 27.7°$, and we arbitrarily considered 100 lipid molecules over the range of θ angles. The CSA of ^{31}P, the B_0 field strength, the QC parameters of ^{2}H sites in a palmitoyl chain, and the line broadening factors considered for the spectral simulations are 32 ppm, 7.05 T, 4–32 kHz, and 50–200 Hz, respectively. Distorted peaks are visible in both ^{31}P and ^{2}H ssNMR spectra at $d/a \neq 0$ when a slow lateral diffusive rate ($D_{ld} = 10^{-10}$ cm^2/s) is considered (middle row). This is because a single sharp peak (^{31}P) or a pair of sharp peaks (^{2}H) resulting from a site in a perfectly aligned lipid bilayer ($d/a = 0$; top row) is distorted and broadened due to the disorder produced in a thinned dimple. If lipids migrate from one region to another by a fast lateral diffusion, ca., $D_{ld} = 5\times10^{-7}$ cm^2/s, a motionally averaged single sharp peak (^{31}P) or pair of sharp peaks (^{2}H) per site will be obtained at the center-of-mass position of an anisotropic frequency span of a site, resulting in apparently reduced ^{31}P CSA and ^{2}H QC tensor parameters (bottom row). Therefore, the magnitudes of the apparent ^{31}P CSA and ^{2}H QC tensor parameters obtained from the spectra of lipids, distributed on a thinned surface with a fast lateral diffusion coefficient, decrease as the d/a ratio increases. In many cases, thinned membrane bilayers would be formed prior to the formation of pores in lipid membranes (carpet model). Thus, in actual AMP–lipid interaction systems, lipid pores formed by the insertion of AMPs in membranes would be located in membrane bilayers that are already thinned.

Fig. 3 shows ^{31}P (B–D) and ^{2}H (E–G) ssNMR spectral lineshapes of POPC-d_{31} lipid bilayers forming toroidal pores of $d = 0.5b$ (B, E), $d = b$ (C, F), and $d = 1.4b$ (D, G), with lateral diffusion coefficients $D_{ld} = 10^{-8}$ cm^2/s, 10^{-9} cm^2/s, 10^{-10} cm^2/s, and 10^{-11} cm^2/s. The peak intensity along the 0° orientation overwhelms the peak intensity along the 90° orientation in both ^{31}P and ^{2}H spectra when $d/b > 1$ (D and G), while the opposite trend is the case when $d/b < 1$ (B and E). The pore radius, a, was fixed to the monolayer thickness, b (= 20 Å), of a lipid bilayer [19,64,65]. It has been reported that about 90 POPC lipids are involved in a pore induced by magainin-2 [45,66]. In the simulations however, we arbitrarily used 100 anisotropic orientations of lipid molecules with the same tensor values and spectral processing parameters as used for the spectra shown in Fig. 2. It must be noticed that the line broadening factors (50–200 Hz) used for the spectral processing cannot explain the extent of peak broadening/coalescent effects introduced in the simulated ^{31}P and ^{2}H spectra.

A simple line broadening effect is visible when the diffusion coefficient D_{ld} is slower than 10^{-10} cm^2/s. Most of the detailed fine structures of ^{31}P and ^{2}H spectra are washed away when D_{ld} is about 10^{-9} cm^2/s. When D_{ld} reaches the 10^{-8} cm^2/s regime, a lateral diffusion coefficient of pure lipids, we observe motionally averaged ^{31}P and ^{2}H NMR spectra, with shifted center-of-mass positions depending on the ratio of d/b. The center-of-mass positions of two anisotropic ^{2}H spectra of lipids on an elliptic pore per each ^{2}H site do not coincide in general, and the gap between the center-of-mass positions of two transitions becomes wider as the QC tensor parameter or the d/b ratio increases (Fig. 3F and G). At $d = 0.5b$, however, all ^{2}H peaks provide a coinciding center-of-mass position regardless of the magnitude of QC parameters, resulting in a single sharp peak at the center with $D_{ld} = 10^{-8}$ cm^2/s (Fig. 3E). At this condition, both ^{31}P and ^{2}H anisotropic spectra are somewhat similar to those from lipids that take a random, a micellar, or a liposomal distribution. However, unlike those spectra from a random or a spherical distribution, anisotropic lineshapes of ^{31}P and ^{2}H NMR spectra of lipids distributed on an elliptic pore with $d/b = 0.5$ that are simulated at $z // B0$ and z B_0 orientations are distinctive [43]. These motionally averaged, spectral broadening/coalescent effects are evidenced experimentally in ^{31}P and ^{2}H ssNMR spectra measured on oriented POPC membranes interacting with the antimicrobial peptide protegrin-1 [43,46].

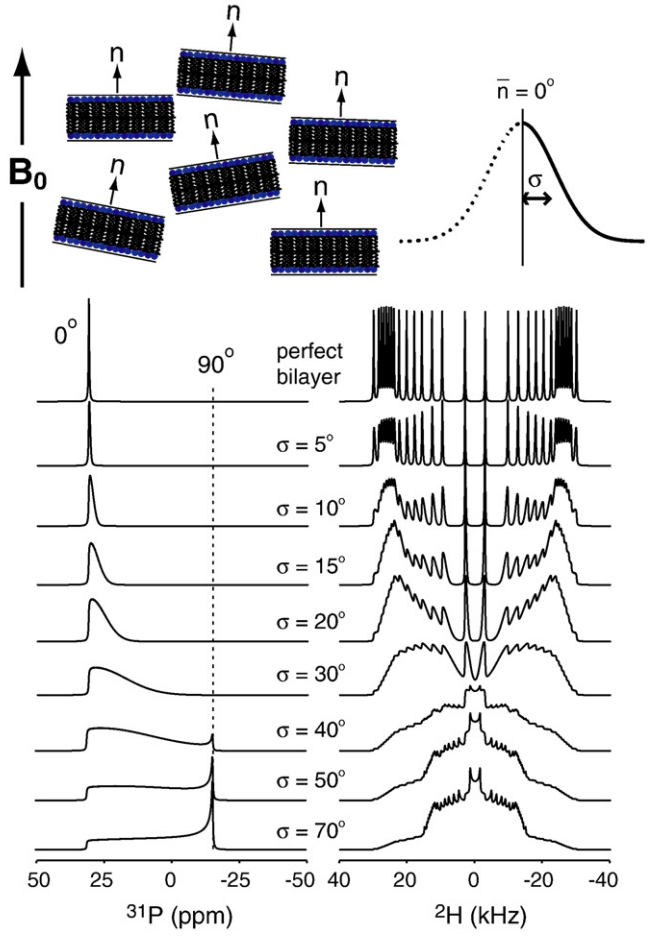

Fig. 4. ^{31}P and ^{2}H lineshapes expected from lipid bilayers whose bilayers' normal directions are spreaded by mosaic distribution with $\sigma = 5$–70°. When the average of the bilayers' normal directions is placed parallel to the applied magnetic field, the rotational invariance around the magnetic field direction, B_0, makes the lineshapes resulting from the mosaic distribution of bilayers half-Gaussian shapes. The known range, $\sigma = 5$–15°, of mosaic spread of oriented phospholipids prepared between glassplates still provides relatively narrow, asymmetrically broadened lines in ^{31}P and ^{2}H spectra around 0° position, the average bilayer normal direction. Even under a seriously distorted distribution with ca. $\sigma = 30°$, non-realistically broadened lines in ^{31}P and ^{2}H spectra still lack peak intensities around the 90° position. When σ exceeds 50°, the distorted lineshapes for both ^{31}P and ^{2}H spectra resemble a rather the lineshape from a random lipid distribution.

It should be noticed that the anisotropic ^{31}P and ^{2}H ssNMR lineshapes based on a toroidal pore model are completely distinguishable from the lineshapes expected from lipid bilayers spreaded discontinuously by the mosaic distribution [67]. In a fluid mosaic model, the bulk of the phospholipids are arranged in discontinuous, fluid bilayers, whose membrane normal directions are scattered around an average value. As distortions are introduced in a perfect bilayer, anisotropic disorders will be reflected in frequency positions away from the 0° position toward the 90° position, which are positioned at the leftmost and rightmost in the frequency span, respectively. This is because only a change in the polar angle, not the azimuthal angle (only when $\eta = 0$) and the positional rotation around the external magnetic field direction B_0, contributes to a frequency shift in a NMR spectrum. As shown in Fig. 4, an asymmetric resonance line would result from discontinuous bilayers whose membrane normal directions are taking a Gaussian distribution, with a standard deviation σ, around an average direction, which is chosen to be parallel to the applied external magnetic field direction B_0. It was

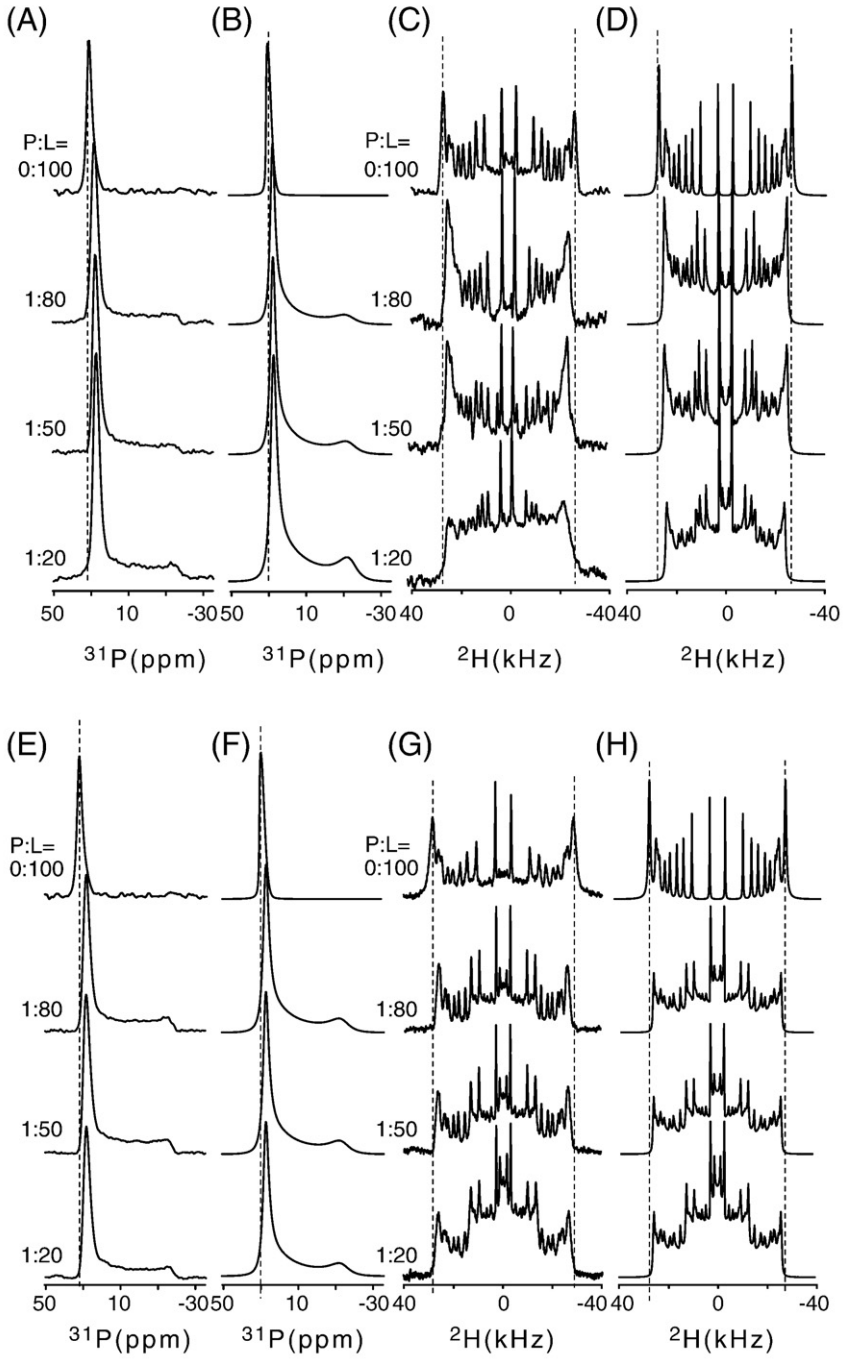

Fig. 5. Experimental (A, C, E, G) and simulated (B, D, F, H) ^{31}P (A, B, E, F) and ^{2}H (C, D, G, H) ssNMR spectra of oriented POPC-d_{31} bilayers prepared between thin cover-glass plates, interacting with magainin-2 (A–D) and aurein-3.3 (E–H) at P:L ratios 0:100, 1:80, 1:50, and 1:20. The glassplate normal was placed parallel to the applied magnetic field direction ($z//B_0$) for NMR measurements. Eye-guides are drawn by dashed lines along the 0° orientation of lipids in the spectra of the pure lipid system for monitoring the decrease in the linewidth at different peptide concentrations. Both ^{31}P and ^{2}H ssNMR spectra measured at all P:L ratios conform to the spectral simulations based on an elliptic toroidal pore model with variable d/b ratios. The observed decreases in the frequency spans of ^{31}P and ^{2}H ssNMR spectra evidence thinned membrane bilayers with fast moving lipids ($D_{ld} = 10^{-8}$–10^{-9} cm^2/s). The ^{2}H spectra of aurein-3.3 showed elliptic pores with shorter d lengths (perhaps due to deeper peptide insertions) than those cases involving maginin-2, while providing less prominent thinning effects, even at P:L = 1:20. The potential portion of lipids that keeps flat membrane bilayers is not considered in the simulations.

reported that oriented lipid bilayers prepared between cover-glass plates have mosaic spreads of $\sigma = 5$–$15°$ [47,67]. Included in Fig. 4 are ^{31}P and ^{2}H ssNMR lineshapes expected for lipid bilayers having mosaic spreads of $\sigma = 5$–$70°$. As can be seen in either ^{31}P or ^{2}H spectrum shown in Fig. 4, even a very broad, asymmetrical lineshape with $\sigma = 30°$ does not provide anisotropic frequencies near 90°. When the σ exceeds 40°, those severely distorted lineshapes shown in Fig. 4 approach a rather that of a random distribution.

4. Experimental results

4.1. Interaction of magainin-2 and aurein-3.3 with POPC bilayers

A zwitterioninc type of membrane lipid, POPC, has a hydrophilic headroup and hydrophobic palmitoyl- and oleyl acyl chains. Zwitterionic lipids are common in membranes of *eukaryotic* cells and, therefore, POPE or POPC can be used as a reference for mixed membrane systems. Using ^{31}P and ^{2}H ssNMR spectroscopy, we studied oriented POPC-d_{31} bilayers binding with magainin-2 and aurein-3.3 at various peptide:lipid (P:L) ratios. Fig. 5 shows experimental (A, C, E, and G) and simulated (B, D, F, and H) ^{31}P (A, B, E, and F) and ^{2}H (C, D, G, and H) ssNMR spectra of oriented POPC-d_{31} bilayers interacting with magainin-2 (A–D) and aurein-3.3 (E–H), at peptide-to-lipid (P:L) ratios 0:100, 1:80, 1:50, and 1:20. A stack of glass plates is placed in the external magnetic field B_0 so that the glass plate normal is parallel to the external magnetic field B_0 ($z // B_0$). An ideal lipid bilayer would provide peaks only along the 0° orientation in the absence of AMPs. An asymmetrical lineshape in ^{31}P spectrum at P:L = 0:100 would exemplify potentially possible mosaic spreads of lipid bilayers with $\sigma \approx 10°$. As AMPs perturb membrane structures, we observe distorted lineshapes spanning over the entire frequency range from 0° to 90° position in ^{31}P and ^{2}H ssNMR spectra, even at P:L = 1:80. Interestingly, the observed ^{31}P and ^{2}H spectral lineshapes are not able to be explained by considering a mosaic spread model because a mosaic distribution model does not generate frequencies spanning over all the anisotropic frequency positions, including the frequency around the 90° position, without providing a significantly broadened lineshape along the 0° position (see Fig. 4); nor are lineshapes congruent with a random model either (see Fig. 1B). However, these lineshapes can be simulated well by a toroidal pore model with variable d values (see Fig. 3) as shown in Fig. 5. The observed NMR tensor parameters agree with the known values for phospholipids in liquid crystalline states [45–47] ($\delta_{csa} = 30$ ppm, $\eta_{csa} = 0$ for the ^{31}P CSA, and $e^2qQ/\hbar = 3.0$–36 kHz and $\eta_{QC} = 0$ for ^{2}H QC parameters (see Table 1)). The quadrupolar splittings are characterized by the mobility of the CD_2 groups in the acyl chains of lipids. The formation of a lipid pore imposes anisotropic line broadenings in both ^{31}P and ^{2}H spectra without modifying tensor parameters that are determined in pure lipid bilayers [68,69]. ^{31}P CSA and ^{2}H QC tensor parameters associated with various types of lipid topologies can be extracted either by direct spectral simulations or signal dePaking [70].

The best-fit simulations in Fig. 5 (B, D, F, and H), incorporating a pore model over the P:L ratios from 1:80 to 1:20, were provided by ranges of d values from $1.5b$–$1.8b$ to $1.0b$–$1.2b$, respectively, with $a = b$. The dimension of a is arbitrary, however, we have used $a = b$ in our simulations for simplicity, based on the experimental observation that the range of pore diameters induced in the cell membranes of *Escherichia coli* interacting with cecropin is about the monolayer thickness b of bilayers [71]. The amount of the lateral diffusion coefficient of lipids cannot be assessed from these 1D spectra because the influence of lateral diffusive motions of lipids is not exemplified in the spectra. By comparing to the simulated spectra, however, we can be assessed that it is slower than 10^{-11} cm^2/s. The observed spin–spin relaxation time, T_2, of ^{31}P in phospholipids is in the 0.5–1.4 ms range over the peptide concentrations we tested. Although it is not explicitly included in the simulated spectra, the lineshape of a potentially flat portion of lipid bilayers, with some degree of mosaic spread, can be added to the pore lineshape, producing more intense signal intensity along the 0° position. As the peptide concentration increases, the observed trend in the spectra, particularly in ^{2}H spectra of the POPC-

Table 1
^{31}P CSA and ^{2}H QC tensor parameters of POPC-d_{31} and/or POPG lipids in various AMP–lipid compositions.

AMP: lipid	CSA[a]	1[b,c]	2	3	4	5	6	7	8	9	10	11	12	13	14	15[d]
PC[e]	33	38.3	38.3	38.2	38.1	37.9	36.6	34.7	34.0	32.0	28.6	26.3	22.3	18.7	14.2	4.2
MG[f]:PC = 1:80	32	33.6	33.6	33.5	33.4	33.2	32.1	30.4	28.0	26.2	23.2	21.2	18.6	15.5	11.5	3.68
MG:PC = 1:50	32	33.0	33.0	32.9	32.8	32.7	31.6	29.9	26.6	24.9	21.9	19.9	16.5	14.3	10.4	3.53
MG:PC = 1:20	32	31.8	31.8	31.7	31.6	31.4	30.4	28.7	25.1	23.5	20.6	18.7	15.8	13.7	10.4	3.39
AU[g]:PC = 1:80	32	35.4	35.4	35.3	35.2	35.0	33.9	32.0	31.4	29.6	26.4	24.3	20.6	17.3	13.1	3.9
AU:PC = 1:50	32	35.4	35.4	35.3	35.2	35.0	33.9	32.0	31.4	29.6	26.4	24.3	20.6	17.3	13.1	3.9
AU:PC = 1:20	32	34.7	34.7	34.6	34.5	34.3	33.2	31.4	30.8	29.0	25.8	23.8	20.1	16.9	12.8	3.8
PC(3)/ PG[h](1)	35	36.5	36.5	36.4	36.3	36.1	34.9	33.0	32.4	30.5	27.2	25.0	21.2	17.8	13.5	4.00
MG:PC(3)/ PG(1) = 1:80	34	32.9	32.9	32.8	32.7	32.5	31.4	29.7	28.3	26.6	23.6	21.6	17.8	16.0	12.2	3.60
MG:PC(3)/ PG(1) = 1:50	34	31.8	31.8	31.7	31.6	31.4	30.4	28.7	26.4	24.8	21.9	20.0	17.0	14.4	10.6	3.48
MG:PC(3)/ PG(1) = 1:20	34	27.0	27.0	26.9	26.6	26.5	25.5	24.2	21.5	20.1	17.6	16.0	13.4	11.5	8.29	2.96
AU:PC(3)/ PG(1) = 1:80	32	37.5	37.5	37.3	37.2	36.6	35.4	34.0	32.8	29.8	27.2	25.0	21.2	17.9	13.5	4.00
AU:PC(3)/ PG(1) = 1:50	31	36.4	36.4	36.4	36.3	36.2	35.5	33.9	32.0	31.4	29.6	26.4	24.3	20.6	17.4	13.1	3.88
AU:PC(3)/ PG(1) = 1:20	31	31.9	31.9	31.8	31.7	31.1	29.7	26.4	25.8	24.2	21.4	19.6	16.3	14.3	10.5	3.40
PC(1)/ Chol[i](1)	28	67.0	66.5	66.0	65.6	65.0	64.0	62.0	61.0	57.5	57.2	53.8	48.5	41.0	31.0	8.20
MG:PC(1)/ Chol(1) = 1:80	27	65.1	65.1	65.0	64.8	63.8	62.8	61.7	59.9	58.1	53.0	48.4	43.4	35.5	26.6	7.20
MG:PC(1)/ Chol(1) = 1:50	27	65.1	65.1	65.0	64.8	63.8	62.8	61.7	59.9	58.1	53.0	48.4	43.4	35.5	26.6	7.20
MG:PC(1)/ Chol(1) = 1:20	27	57.9	57.9	57.8	57.1	56.8	55.0	54.0	50.6	48.6	47.2	44.9	38.6	31.6	23.6	6.41
AU:PC(1)/ Chol(1) = 1:80	28	65.1	65.1	65.0	64.8	63.8	62.8	61.7	59.9	58.1	53.0	48.4	43.4	35.5	26.6	7.20
AU:PC(1)/ Chol(1) = 1:50	28	63.8	63.8	63.7	63.5	62.5	61.5	60.5	58.7	56.9	51.9	47.4	42.5	34.8	26.0	7.06
AU:PC(1)/ Chol(1) = 1:20	28	56.6	56.6	56.6	56.4	55.5	54.6	53.7	52.1	50.5	46.1	42.1	37.8	30.9	23.1	6.26

[a] Chemical shift anisotropy of ^{31}P in ppm ($\delta_{csa} = \delta_{//} = \delta_{22}$; $\eta = 0$; $\delta = (\delta_{11} + \delta_{33})/2$).
[b] Quadrupolar coupling constants ($e^2qQ/$) of ^{2}Hs in the palmytoyl chain of POPC-d_{31} (kHz).
[c] Numbers represent the positions of CD_2 groups separated from the carbonyl of palmytoyl chain.
[d] The terminal CD_3 group of palmytoyl chain.
[e] POPC-d_{31}.
[f] magainin-2.
[g] aurein-3.3.
[h] POPG.
[i] Cholesterol.

d_{31}/aurein-3.3 system, is the spectral feature of a pore model with shorter d length. However, the trend in the ^{31}P spectra is not as prominent as that of the ^{2}H spectra. Aurein-3.3 produces pores with somewhat shorter d lengths than magainin-2 as can be seen in the spectra. Based on the best-fit simulation data, the simulated d values that agree with the features of experimental spectra are 1.8b (P:L = 1:80), 1.7b (P:L = 1:50), and 1.5b (P:L = 1:20) for magainin-2/POPC-d_{31} and 1.2b (P:L = 1:80), 1.1b (P:L = 1:50), and 1.0b (P:L = 1:20) for aurein-3.3/POPC-d_{31}. The tensor parameters of ^{31}P CSA and ^{2}H QC interactions obtained from the best-fit simulations are provided in Table 1.

Another feature observed is the decrease in the frequency spans of both ^{31}P and ^{2}H ssNMR spectra in Fig. 5 as the peptide concentrations increase. This phenomenon is more prominent in ^{2}H spectra, which measure the hydrophobic environment of peptide–lipid complexes. Although several groups have shown the relationship of the decrease in peak splitting with the changes in membrane thickness [48,72], no theoretical model has been provided yet to explain this phenomenon; however our membrane thinning model considered with a fast lateral diffusion coefficient of lipids successfully explains this property (Fig. 2). The magnitudes of apparent ^{2}H QC tensor parameters observed in Fig. 5 are clearly less than those observed from pure lipid bilayers, particularly at high P:L ratios. According to the best-fit simulation data obtained from the membrane thinning model, the observed decreases in the anisotropic frequency spans of ^{2}H ssNMR spectra of POPC-d_{31}/magainin-2 and POPC-d_{31}/aurein-3.3 produced

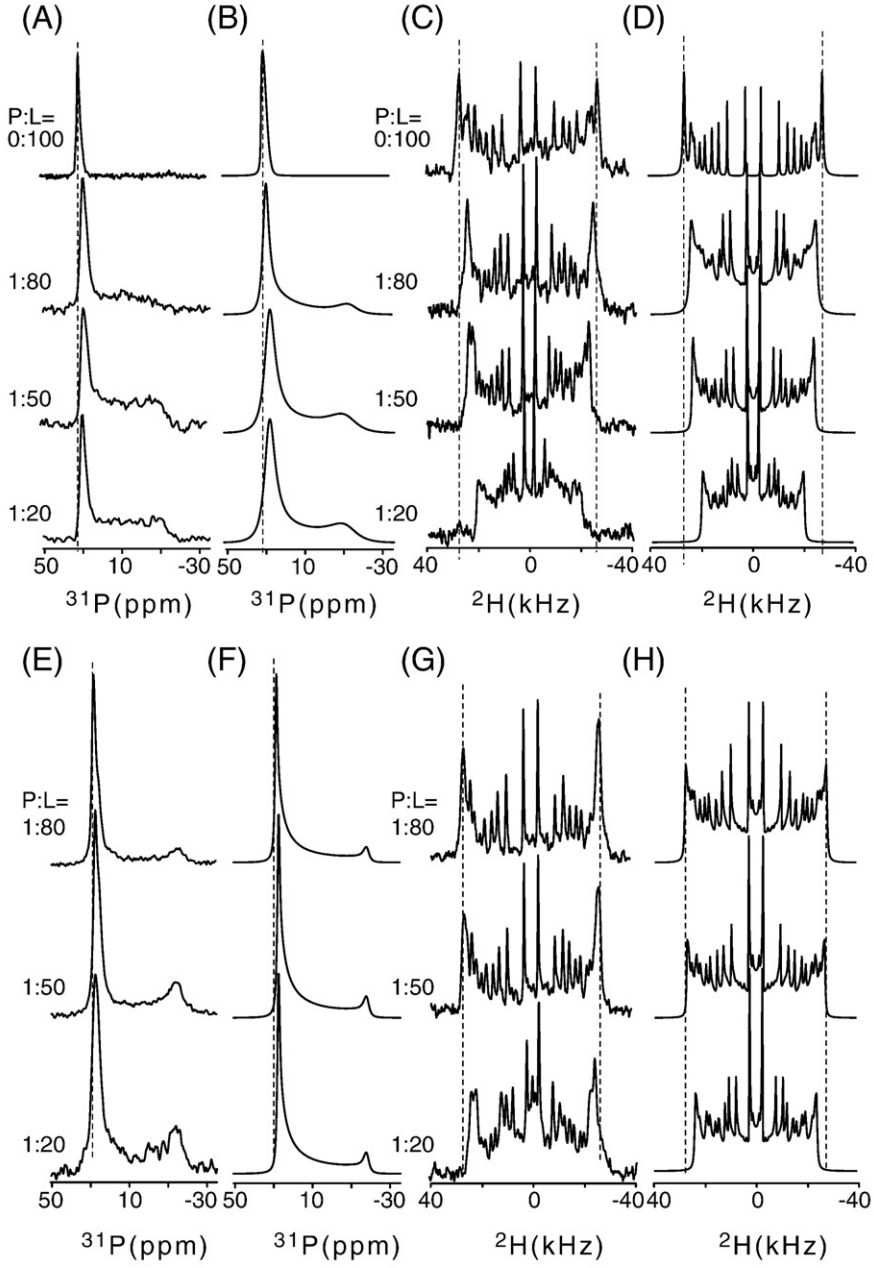

Fig. 6. Experimental (A, C, E, G) and simulated (B, D, F, H) ^{31}P (A, B, E, F) and ^{2}H (C, D, G, H) ssNMR spectra of magainin-2-bound (A–D) and aurein-3.3-bound (E–H) POPC-d_{31}/POPG (molar ratio = 3:1) membrane bilayers that are oriented between thin cover-glass plates ($z//B_0$). Peptide-to-lipid ratios considered are P:L = 0:100, 1:80, 1:50, and 1:20. The presence of anionic POPG lipids provides a significantly prominent membrane thinning effect in the ^{2}H spectra at high peptide-to-lipid ratios. The membrane thinning effect observed in the ^{2}H spectra of the aurein-3.3 system is less prominent than the case involving magainin-2. The shoulder peak near the 0° orientation in the ^{31}P spectra of the aurein-3.3 system at all P:L ratios might indicate a portion of thinned membranes with a slower lateral diffusive rate that maintains the same geometrical feature, or a portion of thinned surfaces with a bigger d/a ratio that maintains the same lateral diffusive rate.

$d/a = 0.1$–0.2 and $D_{ld} = 10^{-7}$–10^{-8} cm^2/s. In our experimental spectra, the relative portions of lipids that are involved in pores and thinned membranes are unclear.

4.2. Interaction of AMPs with anionic membranes

Anionic lipids, which are abundant in *prokaryotic* cell membranes, are crucial for the mode of interaction for cationic AMPs to selectively bind on the bacterial cell membrane. An electrostatic interaction between anionic lipids and cationic AMPs plays a central role for antimicrobial action. We incorporated a lipid system consisting of a POPC and POPG mixture with a molar ratio of 3:1 to mimic the non-neutral lipid composition of the bacterial cell membranes in a simple way. Fig. 6 shows experimental (A, C, E, G) and simulated (B, D, F, H) ^{31}P (A, B, E, F) and ^{2}H (C, D, G, H) ssNMR spectra of POPC-d_{31}(3)/POPG (1) lipids interacting with magainin-2 (A, B, C, D) and aurein-3.3 (E, F, G, H), at P:L ratios 0:100, 1:80, 1:50, and 1:20. In these peptide–lipid systems containing anionic lipids the frequency span of ^{2}H spectra decreases prominently, as can be identified clearly from the samples with P:L = 1:20, as the peptide concentration increases (Table 1). The observed ^{31}P CSA tensor parameters, however, are still very similar to those obtained without anionic POPG lipids as listed in Table 1.

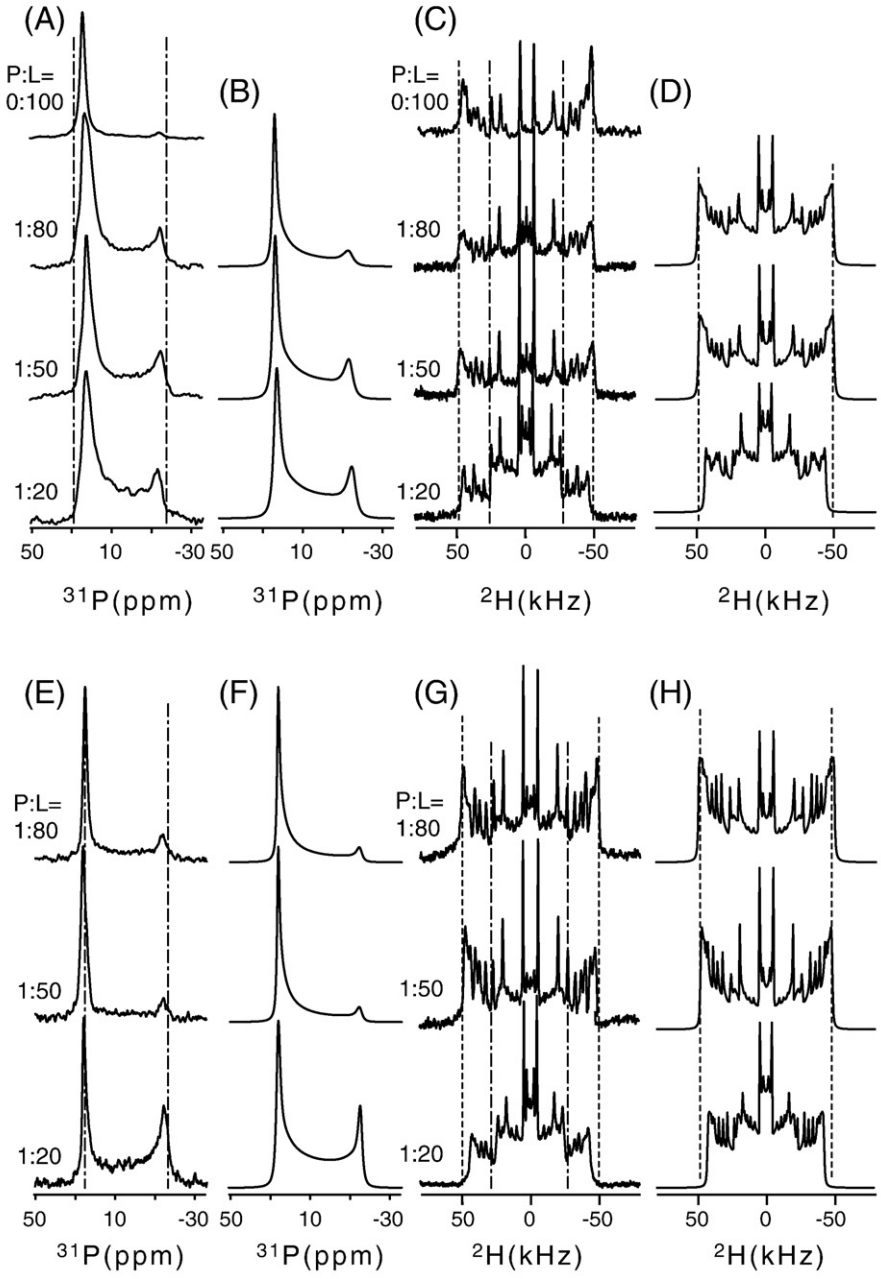

Fig. 7. Experimental (A, C, E, F) and simulated (B, D, F, H) ^{31}P (A, B, E, F) and ^{2}H (C, D, G, H) ssNMR spectra of magainin-2-bound (A–D) and aurein-3.3-bound (E–H) POPC-d_{31}/cholesterol (molar ratio = 1:1) membrane bilayers measured at $z//B_0$. Peptide-to-lipid ratios considered are P:L = 0:100, 1:80, 1:50, and 1:20. Pore forming and thinning phenomena are visible in both ^{31}P and ^{2}H spectra. Eye-guides with dashed and dashed-dot lines compare the size of frequency spans at different P:L ratios and indicate the frequency spans of peptides with POPC-d_{31} lipids without cholesterol, respectively. Unlike the ^{31}P spectra, the frequency spans of ^{2}H spectra of POPC-d_{31} lipids involving cholesterol increased significantly, revealing decreased segmental motions of hydrophobic acyl chains. The length d of the simulated pore geometry decreases as the peptide concentration increases. The spectral features of ^{2}H spectra of aurein-3.3 system are quite similar to those from magainin-2, except the fact that pores induced in membranes possess somewhat longer d values. Notice the decrease in the linewidth of ^{31}P spectra at all P:L ratios.

When a toroidal pore model is incorporated, the anisotropic ^{31}P and ^{2}H ssNMR spectra of POPC-d_{31}(3)/POPG(1) lipids interacting with magainin-2 and aurein-3.3 peptides again provide lineshape characteristics that are consistent with toroidal pores with $a \approx b$ and $d = 1.6$–$1.8b$. The potential contribution from the flat portions of lipid bilayers is not explicitly included in the simulated spectra. Except for the prominent linewidth decrease observed in ^{2}H spectra, magainin-2 does not provide much difference in the shape of pores induced in the POPC-d_{31} lipids, both with and without the presence of POPG lipids, at all three P:L ratios. However, a dramatic increase in d values, from 1.0–1.2b to 1.6–1.8b, is observed in the lipids interacting with aurein-3.3 as the lipid composition changed from pure POPC-d_{31} to POPC(3)/POPG(1). Both peptides, however, show very similar spectral characteristics in ^{31}P NMR spectra for both POPC and POPC(3)/POPG(1) lipid systems even at P:L = 1:20. The lateral diffusion coefficients incorporated in the pore lineshape simulations for the experimental ^{31}P and ^{2}H ssNMR spectra of both peptide systems are $D_{ld} \leq 10^{-11}$ cm^2/s because we do not observe any motionally averaged lineshapes. However, the range of lateral diffusion coefficients required for explaining the membrane thinning phenomenon is $D_{ld} = 10^{-7}$–10^{-8} cm^2/s as explained previously.

4.3. Interaction of AMPs with POPC/cholesterol

Cholesterol is an important constituent of *eukaryotic* cell membranes which is generally absent from bacterial membranes. Cholesterol is largely hydrophobic, but it has one polar group, a hydroxyl, making it amphipathic, allowing its insertion into a membrane bilayer with the hydroxyl group oriented toward the aqueous phase and the hydrophobic ring system faced to the fatty acid tails of phospholipids. Cholesterol immobilizes the first few acyl chains of the phospholipids, making lipid bilayers less deformable and less permeable to small water soluble molecules including AMPs [73–75].

We prepared 1:1 mixture of POPC-d$_{31}$ and cholesterol to investigate the influence of cholesterol in AMP–lipid interactions. Fig. 7 shows experimental (A, C, E, G), and simulated (B, D, F, H) ^{31}P (A, B, E, F) and ^{2}H (C, D, G, H) ssNMR spectra of POPC-d_{31}/cholesterol (1:1 molar ratio) interacting with magainin-2 (A, B, C, D) and aurein-3.3 (E, F, G, H) at P:L ratios of 0:100, 1:80, 1:50, and 1:20. Dashed–dot lines provided in ^{31}P and ^{2}H spectra (in A, C, E, and G of Fig. 7) are eye-guides which indicate the frequency spans of the spectra measured without cholesterol (Fig. 5). Dashed lines provided in the ^{2}H spectra are eye-guides indicating decreases of the linewidth as the peptide concentration increases, which can be attributed to a membrane thinning effect as explained previously. Based on our simulation, the lineshapes of both ^{2}H and ^{31}P spectra evidence the presence of induced lipid pores with $d > b$ in oriented membranes of both sample systems. The pore parameters obtained from the best-fit simulations are $d = 1.5b$ (P:L = 1:80), $d = 1.2b$ (P:L = 1:50), and $d = 1.1b$ (P:L = 1:20) for POPC-d_{31}/cholesterol/magainin-2 and $d = 1.6b$ (P:L = 1:80), $d = 1.5b$ (P:L = 1:50), and $d = 1.0b$ (P:L = 1:20) for POPC-d_{31}/cholesterol/aurein-3.3, assuming $a = b$.

^{2}H spectra from both peptide systems demonstrate dramatic increases of the QC parameters of all ^{2}H sites (Table 1). This feature agrees with the fact that cholesterol molecules that are inserted into membranes freeze the segmental motion of hydrophobic acyl chains of lipids, resulting in the increase of ^{2}H's QC tensor parameters. The QC parameters obtained from both sample systems were in the range of 7.2–65 kHz depending on the position of the ^{2}H site in the palmitoyl chain. However, the CSA parameters of ^{31}P nuclei are in the range of 27–28 ppm, which are actually less than the value observed at the pure POPC lipid system without cholesterol, indicating that the presence of cholesterol does not deter the rates of uniaxial rotations of POPC lipids.

5. Discussion

Maganinin-2, an AMP with 23 amino acid residues, forms an α-helical structure in lipid membranes [76]. In a helical wheel representation, it makes an amphipathic helix with well-defined hydrophobic (red) and hydrophilic (blue) faces, as shown in Fig. 8A. The secondary structure of the aurein-3.3 peptide in lipid membranes is still unknown. In a helical wheel representation as shown in Fig. 8B, however, aurein-3.3 also reveals well-separated hydrophobic and hydrophilic faces, suggesting that aurein-3.3 would form an α-helical structure in lipid membranes.

The positively charged residues located on the hydrophilic face of a helix would be faced-up, allowing favorable electrostatic interactions with the anionic headgroups of lipids, while the hydrophobic residues on the opposite side would be faced-down and buried into the membrane, contacting the hydrophobic tail groups of lipids (Fig. 9A) [77]. This mode of AMP–lipid interaction would facilitate thinned membrane bilayers, a common feature when the peptide concentration is low. After reaching a critical AMP concentration, a few closely placed AMP molecules would self-assemble into a bundle while angling and inserting into the membrane to form a toroidal wormhole (Fig. 9B) [78]. This mechanism explains reasonably well the formation of a toroidal pore with variable length d with respect to b (Fig. 3), which is required to explain most of our ^{31}P and ^{2}H ssNMR spectra measured on lipids interacting with magainin-2 and aurein-3.3. By forming a deeply inserted bundle in the membrane, cationic AMPs would find a favorable way to coexist with amphiphilic lipids and water molecules as shown in Fig. 9C. It allows water molecules inside of the pore to transport molecules and ions across the membrane. ^{31}P and ^{2}H ssNMR spectra with variable 0°/90° intensities satisfying a toroidal pore model with variable length d were frequently observed at various P:L ratios when β-hairpin shaped, defensin-like (cysteine-rich) AMPs or α-helical structured AMPs were interacting with oriented phospholipids [43,46]. A toroidal pore model considering different d lengths (Figs. 3B–G) successfully explains different types of experimental ^{31}P and ^{2}H ssNMR lineshapes exhibiting variable intensities between the 0° and 90° positions of lipids [43,46].

The type shown in Fig. 9D could also be a plausible model to explain the insertion of a bundle of self-assembled AMPs in the membrane. In this case, peptides hide hydrophobic residues (black) inside of the bundle, while exhibiting hydrophilic residues (red) outside, to favor interactions with hydrophilic headgroups of lipids and water. In this model, lipids located on the inner surface of a pore would be more flexible for lateral diffusivity than the case shown in Fig. 9C because peptides are not intermingled with lipid molecules on the pore wall by penetration. However, this type would be less

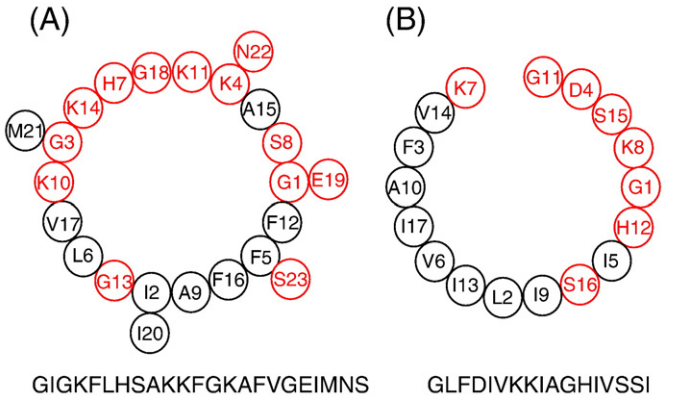

Fig. 8. Helical wheel representations of magainin-2 and aurein-3.3 peptides. Both peptides demonstrate well-separated hydrophobic and hydrophilic faces. This may suggest a potential amphipathic helical structure of aurein-3.3 in lipids, as in the case of magainin-2.

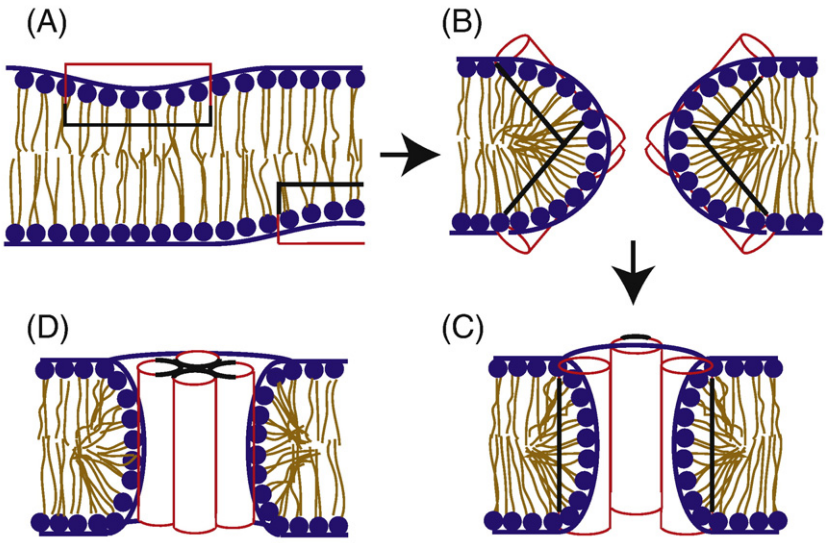

Fig. 9. Models suggested for explaining the gradual insertion of peptides and the formation of elliptic toroidal pores with variable *d* length. AMPs bound on the membrane surface (A) self-assemble and tilt in order to insert into the membrane (B). AMPs insert deeper into the membrane to form a well-defined pore and accommodate molecular/ionic transportations across the membrane through this pore (C). Also plausible is a model assuming a self-assembled peptide bundle, with hydrophobic faces buried inside of the bundle, which can be inserted into a bilayer to form a pore (D). The outward-facing hydrophilic faces of the peptide bundle make favorable interactions with the hydrophilic headgroups of lipids.

favorable for an efficient transportation of molecules or ions through the pore compared to the other type shown in Fig. 9C because the inside part of the pore that is occupied by AMPs is hydrophobic. For cationic AMPs to interact with zwitterionic and neutral lipids, such as POPC or POPC/cholesterol, AMPs would self-assemble into a bundle more readily even at lower AMP concentration to minimize the accumulation of overall charge density. In this case, the critical peptide concentration for the formation of a peptide bundle will be lower than the case involving anionic lipids. On the molecular level, cationic AMPs are readily miscible with anionic lipids but not with zwitterionic lipids.

^{31}P and ^{2}H ssNMR spectroscopic techniques are optimal for diagnosing the structural perturbations in lipid bilayers induced by membrane-acting peptides. Within our knowledge, without incorporating a toroidal pore model with variable length in *d*, it is not possible to explain the lineshape patterns of ^{31}P and ^{2}H ssNMR spectra we obtained experimentally, particularly the intensity profiles along the 90° position with respect to the applied magnetic field direction ($z//B_0$). As can be seen in Fig. 5, the best-fit simulations for the experimentally observed ^{31}P and ^{2}H ssNMR spectra originating from magainin-2/POPC-d_{31} and aurein-3.3/ POPC-d_{31} systems were provided by a toroidal pore model with $a \approx b$, $d > b$, and lateral diffusion coefficients in the range of $\leq 10^{-11}$ cm^2/s—lineshape characteristics that are motionally averaged by lateral diffusions are not visible. The observed pore lineshape characteristics are evident even at the lowest peptide concentration (P:L = 1:80) we considered, indicating that the critical peptide concentration for membrane insertion is very low. However, as the peptide concentration increases, the *d* parameter changes from 1.8*b* (P:L = 1:80) to 1.3*b* (P:L = 1:20) for magainin-2/POPC-d_{31}, and from 1.2*b* (P:L = 1:80) to 1.0*b* (P:L = 1:20) for aurein-3.3/POPC-d_{31}. It is not clear why the *d* parameter of a toroidal pore shows stronger peptide concentration dependence in ^{2}H spectra. We hypothesize however that the insertion of a peptide bundle into a lipid bilayer would result in a more perturbed environment along the hydrophobic tail parts that exist inside of the bilayer than along the hydrophilic headgroups that face outward. We observed that pore lineshapes show time-dependent drift over several days or weeks depending on the composition of membranes (data not shown). Ramamoorthy and coworkers reported that pores initially formed can be converted into micelles or even into inverted hexagonal phases over time [33–35].

In usual cases, thinned membrane bilayers would occur prior to the formation of pores in anionic lipid membranes when interacting with cationic AMPs, because the presence of anionic lipids favors an *S*-bound state over an inserted *I*-state. The helical axis of an α-helical AMP, which takes on a parallel orientation with respect to the surface of a membrane bilayer at low peptide concentrations [18], would need to take on a tilted angle orientation to insert into membranes after a critical concentration has been reached (Fig. 9B). This would explain how a pore with a shallower peptide insertion — an elliptic pore with a longer *d* value — is more likely to be observed with the interaction of a helical AMP with anionic membrane bilayers than with zwitterionic membrane bilayers.

The linewidths of ^{31}P and ^{2}H spectra had decreased prominently in lipid bilayers involving anionic lipids that are interacting with AMPs. The magnitudes of observed coupling parameters of ^{31}P CSA and ^{2}H QC interactions in the presence of AMP molecules are less than those from pure lipid bilayers as summarized in Table 1. Although the linewidth decrease effect is evident both in the ^{31}P CSA and ^{2}H spectra, a more prominent effect was observed in the ^{2}H spectra, which contain local structural and dynamic information of hydrophobic alkyl chains. A synergistic effect between the lateral diffusive motion and the segmental wobbling motion of the hydrophobic acyl chains would provide a more prominent linewidth decrease effect. Interestingly, an increase in the peptide concentration introduced more decreases in the linewidth of both ^{31}P and ^{2}H ssNMR spectra for both peptide cases [58], which can readily be simulated based on our membrane thinning model with a fast lateral diffusive rate of lipids ($D_{ld} = 10^{-7}$–10^{-9} cm^2/s) (Fig. 2). According to our thinning simulation scheme, the observed linewidth decreases in both ^{31}P and ^{2}H anisotropic spectra provide the best-fit simulation with $d/a = 0.2$–0.3 and $D_{ld} = 10^{-8}$–10^{-9} cm^2/s. If we adopt an average thin depth of membranes on the order of 11 Å [58], the diameter of the thinned membrane dimple would be in the range of 36–55 Å.

In general, the lateral diffusive rate of lipids on a membrane surface is a function of the membrane composition, the concentration of an obstacle, temperature, and the hydration level. The lateral diffusion coefficient of lipids in a pure lipid bilayer is 10^{-7}–10^{-8} cm^2/s [79]. In the presence of membrane-acting peptides, the rate of lateral diffusions of lipids in membranes would be slowed down due to the electrostatic, hydrophilic, and/or hydrophobic peptide–lipid interactions. Therefore, membrane surfaces binding with AMPs would have

significantly lower rates of lateral diffusions. Less obvious is why lipids involved in the holes of toroidal pores move more slowly ($<10^{-11}$ cm^2/s) than lipids involved on thinned membrane bilayers (10^{-8}–10^{-9} cm^2/s) if we incorporate our model to explain the linewidth decrease effect. We hypothesize that the lateral diffusive motion of lipids involved in a toroidal pore would be significantly slower than that of pure bilayers because the lipid motion must accompany somewhat unfavorable transbilayer motions involving both up- and down-leaflets (when $z // B_0$, the lateral diffusive motion around ϕ angle is not observable in NMR), while those occurring on a thinned membrane surface would still maintain a reasonably fast diffusive rate because the mechanism involved is the typical lateral diffusive motion of lipids on a single surface. This reasoning matches well with the observation by Opella and coworkers that membrane proteins incorporated in bicelles undergoes fast axial diffusion ($D_{rot} \geq 10^5$ s^{-1}) on the bicelle surface, providing narrow line widths along ^{15}N chemical shift (<2 ppm) and ^{1}H–^{15}N dipolar couplings (~250 Hz) [80].

The range of transverse relaxation time, T_2, measured on POPC, POPC(3)/POPG(1), and POPC(1)/Chol(1) systems interacting with magainin-2 and aurein-3.3 at P:L ratio = 1:80, 1:50, and 1:20 was 0.6–1.5 ms, with shorter T_2 times as the peptide concentration increases (data not shown). Because of these moderate to short T_2 times and the slow lateral diffusive rates of lipids, we cannot attribute the apparent line broadening effect in 1D NMR spectra sorely to the lateral diffusive dynamic motions of lipids. A two-dimensional (2D) exchange spectroscopic technique had been incorporated to investigate slow lateral diffusive rates of lipids. For example, Fig. 10 shows 2D ^{31}P exchange spectra measured on a POPC(3)/POPG(1) system interacting with aurein-3.3 at P:L = 1:20, with mixing times of 5, 50, and 200 ms. As demonstrated in the Figure, at longer mixing times, 50 and 200 ms, peak intensities of experimental spectra centered along the diagonal frequency positions in spectra measured with 5 ms mixing time smeared out to the off-diagonal positions on both sides, demonstrating exchanges among different nuclear sites generating different anisotropic frequencies. This might indicate that nuclear sites possessing different anisotropic frequencies are on the same curved membrane surface. Major peak intensity patterns on the experimental spectra with different mixing times were reasonably well simulated by assuming two-dimensional lateral diffusive motions of lipids located on the curved surface of a pore with $a = b$, $d = 1.6b$, and $D_{ld} = 10^{-11}$ cm^2/s, as shown in Fig. 10D–F. Thus, our postulation to assume mobile lipids on pore surfaces can be justified. Moreover, the order of lateral diffusion coefficients extracted from our lineshape analysis agrees well with other experimental data [81–83].

Even though we consider a potential distribution in the bilayers' normal directions with respect to the glass plate normal direction ($n // B_0$) and assume a few degrees (10–15°) of a typical mosaic spread of lipid bilayers prepared between glass plates [67], which results in an asymmetrical half-Gaussian peak pattern along the frequency position of 0° orientation of lipids (e.g., the peak near 30 ppm in a ^{31}P spectrum), the observed anisotropic frequencies spanning over all the anisotropic frequency regions, including the frequency positions close to and along the 90° orientation (−18 ppm in a ^{31}P spectrum), cannot be explained by this simple mosaic distribution model (see Fig. 4). Moreover, if anisotropic frequencies spanning over the whole spectral range are from discontinuous bilayers that are spread by mosaic distribution, nuclear sites with different anisotropic frequencies

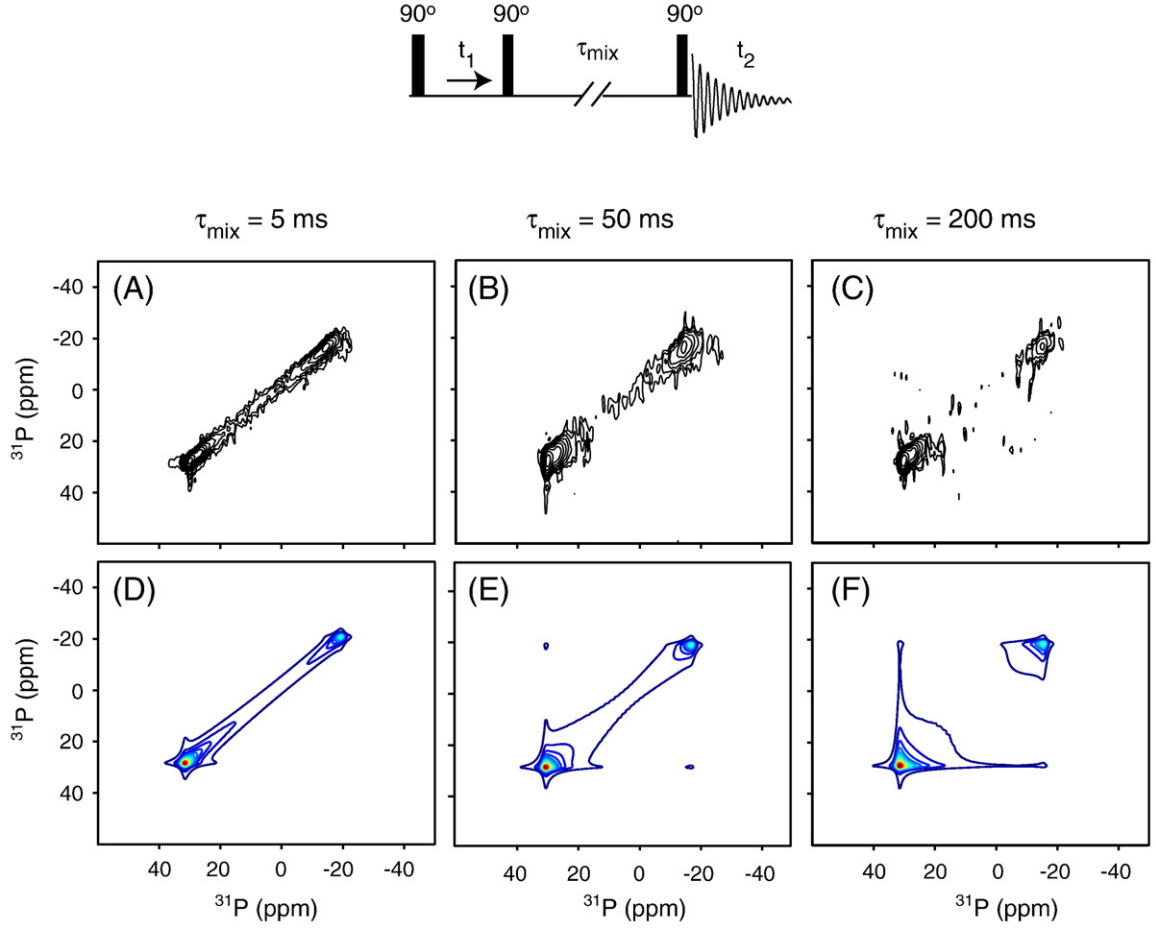

Fig. 10. 2D ^{31}P exchange NMR spectra of POPC (3)/POPG (1) interacting with aurein-3.3 at P:L = 1:20, with mixing times of 5 ms (A), 50 ms (B), and 200 ms (C). The main features of the experimental 2D spectra were reproduced reasonably well by incorporating a pore geometry model with $a = b$, $d = 1.6b$, and $D_{ld} = 10^{-11}$ cm^2/s.

would not provide lateral diffusive exchange among different nuclear sites because they are physically separated.

Several different sizes and shapes of pores and thinned membrane "dimples" would coexist in membranes, and therefore it is more plausible to postulate an ensemble average of these lipid assemblies. So, any AMP-induced lipid pores would be formed in membranes which are already thinned. This might explain why we observe the lineshape characteristics of pores and thinned bilayers simultaneously from the experimental spectra. It is natural to assume that AMPs produce various sizes of pores; however, a significant portion of AMP molecules still maintains *S*-binding states, even at a high peptide concentration, because not all of the AMP molecules are allowed to form peptide bundles. Our experimental spectra measured on POPC, POPC/POPG, and POPC/cholesterol lipids, interacting with magainin-2 and aurein-3.3, support the coexistence of pores with thinned membranes. The relative portions of lipids that are involved in pores and thinned membranes are unclear.

The frequency spans of ^{31}P spectra of POPC/cholesterol lipids interacting with magainin-2 and aurein-3.3 are comparable to those observed without cholesterol, indicating that the presence of cholesterol does not deter the rate of the uniaxial rotation of a lipid around its chain axis. Actually, the frequency spans of ^{31}P spectra of POPC under the interaction of cholesterol show even narrower widths than those spectra without cholesterol at all P:L ratios. This might be explained by considering the increased disorder in lipid bilayers owing to the cholesterol insertion. However, the frequency spans observed in the ^{2}H spectra at all P:L ratios provide dramatic increases in QC parameters at all ^{2}H sites (from 4.0–36.5 kHz without cholesterol to 7.2–65.5 kHz with cholesterol), as shown in Fig. 7 and Table 1. This result satisfies our general expectation that cholesterol molecules that are inserted into membranes freeze the segmental wobbling motions of hydrophobic acyl chains of lipids, resulting in the increase of ^{2}H's QC tensor parameters. This means that the magnitudes of site-specific QC couplings in a perdeuterated acyl chain of a phospholipid that is confined in a lipid bilayer are determined not only by the uniaxial rotation of the lipid around its chain axis, but also by the segmental wobbling motion of its acyl chains. As the peptide concentrations increased, the apparent QC parameters decreased, satisfying our prediction based on the thinning model while demonstrating a transition from elliptic toroidal pores with longer d values to those with shorter d values. For both sample systems, simulations of ^{2}H spectra for all 15 ^{2}H sites in the perdeuterated palmitoyl chain required a lateral diffusion coefficient, $D_{ld} \leq 10^{-11}$ cm^2/s, which is similar to the value obtained from POPC (3)/POPG(1) systems. Based on this observation, we can conclude that cholesterol molecules inserted into membranes do not significantly alter either the rate of either uniaxial rotations or the lateral diffusive rates of lipids, although it freezes the segmental motions of hydrophobic acyl chains. Currently, we are investigating the structures and peptide–peptide associations of AMPs bound on or inserted into membranes by incorporating isotopically labeled AMPs.

6. Conclusion

The main goal of the present study was to investigate the AMP-induced structures and dynamics of supramolecular lipid assemblies induced in oriented bilayers on the molecular level by ssNMR spectroscopy. Anisotropic ^{31}P and ^{2}H ssNMR spectra measured on oriented bilayers of POPC-d_{31}, POPC-d_{31}/POPG, and POPC-d_{31}/cholesterol that are interacting with magainin-2 and aurein-3.3 peptides evidenced the presence of elliptic toroidal pores and thinned membrane bilayers in oriented bilayers. When combined with lateral diffusive dynamics of lipids, these supramolecular lipid assemblies explain well the spectral characteristics of experimental ^{31}P and ^{2}H ssNMR spectra measured on the various lipid systems interacting with magainin-2 and aurein-3.3 at variable P:L ratios. The spectral analysis protocol [43] introduced provides a convenient means to extract the lateral diffusion coefficients of lipids involved on the curved surface of either an AMP-induced pore or a thinned dimple from the lineshape characteristics of motionally averaged ^{31}P and ^{2}H ssNMR spectra that may hitherto have been difficult to characterize. We expect that this protocol would enhance understanding the cell membrane disruptive mechanisms of various types of membrane-acting AMPs.

Acknowledgements

This work is supported by Jeffress Memorial Trust Fund (J-815) and by the NSF (CHE-0541764).

References

[1] M. Papagianni, Ribosomally synthesized peptides with antimicrobial properties: biosynthesis, structure, function, and applications, Biotechnol. Adv. 21 (2003) 465–499.
[2] E. Bachere, Anti-infectious immune effectors in marine invertebrates: potential tools for disease control in larviculture, Aquaculture 227 (2003) 427–438.
[3] B.P. Thomma, B.P. Cammue, K. Thevissen, Mode of action of plant defensins suggests therapeutic potential, Curr. Drug Target Infect. Disord. 3 (2003) 1–8.
[4] R.E. Hancock, R. Lehrer, Cationic peptides: a new source of antibiotics, Trends Biotechnol. 16 (1998) 82–88.
[5] T. Rozek, J.H. Bowie, J.C. Wallace, M.J. Tyler, The antibiotic and anticancer active aurein peptides from the Australian Bell Frogs *Litoria aurea* and *Litoria raniformis*. Part 2. Sequence determination using electrospray mass spectrometry, Rapid Commun. Mass Spectrom. 14 (2000) 2002–2011.
[6] A.M. Cole, Antimicrobial peptide microbicides targeting HIV, Protein and Peptide Lett. 12 (2005) 41–47.
[7] J.M. Conlon, The therapeutic potential of antimicrobial peptides from frog skin, Rev. in Medical Microbiol. 15 (2004) 17–25.
[8] N.Y. Yount, M.R. Yeaman, Immunocontinuum: perspectives in antimicrobial peptide mechanisms of action and resistance, Protein and Peptide Lett. 12 (2005) 49–67.
[9] T. Rozek, K.L. Wegener, J.H. Bowie, N. Olver, J.A. Carver, J.C. Wallace, M.J. Tyler, The antibiotic and anticancer active aurein peptides from the Australian Bell Frogs *Litoria aurea* and *Litoria raniformis*, Eur. J. Biochem. 267 (2000) 5330–5341.
[10] D.W. Hoskin, A. Ramamoorthy, Studies on anticancer activities of antimicrobial peptides, Biochim. Biophys. Acta 1778 (2008) 357–375.
[11] G. Saberwal, R. Nagaraj, Cell-lytic and antibacterial peptides that act by perturbing the barrier function of membranes: facets of their conformational features, structure–function correlations and membrane perturbing abilities, Biochim. Biophys. Acta 1197 (1994) 109–131.
[12] R.E.W. Hancock, T. Falla, M.H. Brown, Cationic bactericidal peptides, Adv. Microb. Physiol. 37 (1995) 135–175.
[13] P. Nicolas, A. Mor, Peptides as weapons against microorganisms in the chemical defense system of vertebrates, Annu. Rev. Microbiol. 49 (1995) 277–304.
[14] J. Nissen-Meyer, I.F. Nes, Ribosomally synthesized antimicrobial peptides: their function, structure, biogenesis, and mechanism of action, Arch. Microbiol., Arch. Microbiol. 167 (1997) 67–77.
[15] M. Edgerton, S.E. Koshlukova, T.E. Lo, B.G. Chrzan, R.M. Straubinger, P.A. Raj, Candidacidal activity of salivary histatins. Identification of a histatin 5-binding protein on *Candida albicans*, J. Biol. Chem. 273 (1998) 20438–20447.
[16] M. Teuber, J. Bader, Action of polymyxin B on bacterial membranes. Binding capacities for polymyxin B of inner and outer membranes isolated from *Salmonella typhimurium G30*, Arch. Microbiol. 109 (1976) 51–58.
[17] P.M. Hwang, H.J. Vogel, Structure–function relationships of antimicrobial peptides, Biochem. Cell Biol. 76 (1998) 235–246.
[18] K. Matsuzaki, Magainins as paradigm for the mode of action of pore forming polypeptides, Biochim. Biophys. Acta 1376 (1998) 391–400.
[19] K. Matsuzaki, K. Sugishita, N. Ishibe, M. Ueha, S. Nakata, K. Miyajima, R.M. Epand, Relationship of membrane curvature to the formation of pores by magainin-2, Biochemistry 37 (1998) 11856–11863.
[20] F. Chen, M. Lee, H.W. Huang, Evidence for membrane thinning effect as the mechanism for peptide-induced pore formation, Biophys. J. 84 (2003) 3751–3758.
[21] B. Bechinger, The structure, dynamics and orientation of antimicrobial peptides in membranes by multidimensional solid-state NMR spectroscopy, Biochim. Biophys. Acta 1462 (1999) 157–183.
[22] Y. Pouny, D. Rapaport, A. Mor, P. Nicolas, Y. Shai, Interaction of antimicrobial dermaseptin and its fluorescently labeled analogues with phospholipid membranes, Biochemistry 31 (1992) 12416–12423.
[23] C. Mazzuca, L. Stella, M. Venanzi, F. Formaggio, C. Toniolo, B. Pispisa, Mechanism of membrane activity of the antibiotic trichogin GA IV: a two-state transition controlled by peptide concentration, Biophys. J. 88 (2005) 3411–3421.
[24] W.T. Heller, A.J. Waring, R.I. Lehrer, H.W. Huang, Multiple states of b-sheet peptide protegrin in lipid bilayers, Biochemistry 37 (1998) 17331–17338.
[25] K. He, S.J. Ludtke, H.W. Huang, Antimicrobial peptide pores in membranes detected by neutron in-plane scattering, Biochemistry 34 (1995) 15614–15618.
[26] Y. Wu, K. He, S.J. Ludtke, H.W. Huang, X-ray diffraction study of lipid bilayer membranes interacting with amphiphilic helical peptides: diphytanoyl phosphatidylcholine with alamethicin at low concentrations, Biophys. J. 68 (1995) 2361–2369.

[27] R.W.S. Glaser, C., U.H.N. Durr, P. Wadhwani, S. Afonin, E. Strandberg, A.S. Ulrich, Concentration-dependent realignment of the antimicrobial peptide PGLa in lipid membranes observed by solid-state 19F-NMR, Biophys. J. 88 (2005) 3392–3397.
[28] S. Afonin, S.L. Grage, M. Ieronimo, P. Wadhwani, A.S. Ulrich, Temperature-dependent transmembrane insertion of the amphiphilic peptide PGLa in lipid bilayers observed by solid state 19F NMR spectroscopy, J. Am. Chem. Soc. 130 (2008) 16512–16514.
[29] E. Strandberg, N. Kanithasen, D. Tiltak, J. Burck, P. Wadhwani, O. Zwernemann, A.S. Ulrich, Solid-state NMR analysis comparing the designer-made antibiotic MSI-103 with its parent peptide PGLa in lipid bilayers, Biochemistry 47 (2008) 2601–2616.
[30] P. Tremouilhac, E. Strandberg, P. Wadhwani, A.S. Ulrich, Conditions affecting the re-alignment of the antimicrobial peptide PGLa in membranes as monitored by solid state 2H-NMR, Biochim. Biophys. Acta, Biomembr. 1758 (2006) 1330–1342.
[31] P. Wadhwani, J. Burck, E. Strandberg, C. Mink, S. Afonin, A.S. Ulrich, Using a sterically restrictive amino acid as a 19F NMR label to monitor and to control peptide aggregation in membranes, J. Am. Chem. Soc. 130 (2008) 16515–16517.
[32] K. He, S.J. Ludtke, W.T. Heller, H.W. Huang, Mechanism of alamethicin insertion into lipid bilayers, Biophys. J. 71 (1996) 2669–2679.
[33] A. Ramamoorthy, S. Thennarasu, D.-K. Lee, A. Tan, L. Maloy, Solid-state NMR investigation of the membrane-disrupting mechanism of antimicrobial peptides MSI-78 and MSI-594 derived from magainin 2 and melittin, Biophysical Journal 91 (2006) 206–216.
[34] S. Thennarasu, D.-K. Lee, A. Tan, U. Prasad Kari, A. Ramamoorthy, Antimicrobial activity and membrane selective interactions of a synthetic lipopeptide MSI-843, Biochimica et Biophysica Acta, Biomembranes 1711 (2005) 49–58.
[35] F. Porcelli, B. Buck, D.-K. Lee, K.J. Hallock, A. Ramamoorthy, G. Veglia, Structure and orientation of pardaxin determined by NMR experiments in model membranes, J. Biol. Chem. 279 (2004) 45815–45823.
[36] M. Zasloff, Magainins, a class of antimicrobial peptides from *Xenopus* skin: isolation, characterization of two active forms, and partial cDNA sequence of a precursor, Proc. Natl. Acad. Sci. U. S. A. 84 (1987) 5449–5453.
[37] M.A. Apponyi, T.L. Pukala, C.S. Brinkworth, M. Maselli, J.H. Bowie, M.J. Tyler, G.W. Booker, J.C. Wallace, J.A. Carver, F. Separovic, J. Doyle, L.E. Llewellyn, Host-defence peptides of Australian anurans: structure, mechanism of action and evolutionary significance, Peptides 25 (2004) 1035–1054.
[38] Y.-L. Pan, J.T.-J. Cheng, J. Hale, J. Pan, R.E. Hancock, S.K. Strauss, Characterization of the structure and membrane interaction of the antimicrobial peptides aurein 2.2 and 2.3 from Australian Southern Bell Frogs, Biophys. J. 92 (2007) 2854–2864.
[39] I. Marcotte, K.L. Wegener, Y.-H. Lam, B.C.S. Chia, M.R.R. de Planque, J.H. Bowie, M. Auger, F. Separovic, Interaction of antimicrobial peptides from Australian amphibians with lipid membranes, Chem. Phys. Lipids 122 (2003) 107–120.
[40] D.J. Hirsh, J. Hammer, L. Maloy, J. Blazyk, J. Schaefer, Secondary structure and location of a magainin analogue in synthetic phospholipid bilayers, Biochemistry 35 (1996) 12733–12741.
[41] B. Bechinger, M. Zasloff, S.J. Opella, Structure and orientation of the antibiotic peptide magainin in membranes by solid-state nuclear-magnetic-resonance spectroscopy, Protein Sci. 2 (1993) 2077–2084.
[42] B. Bechinger, L.M. Gierasch, M. Montal, M. Zasloff, S.J. Opella, Orientations of Helical Peptides in Membrane Bilayers by Solid State NMR Spectroscopy Solid State Nucl, Magn. Reson. 7 (1996) 185–191.
[43] S. Wi, C. Kim, Pore structure, thinning effect, and lateral diffusive dynamics of oriented lipid membranes interacting with antimicrobial peptide protegrin-1: ^{31}P and ^{2}H solid-state NMR study, J. Phys. Chem. B 112 (2008) 11402–11414.
[44] B.A. Cornell, F. Separovic, A.J. Baldassi, R. Smith, Conformation and orientation of gramicidin A in oriented phospholipid bilayers measured by solid state carbon-13 NMR, Biophys. J. 53 (1988) 67–76.
[45] K.J.L. Hallock, MSI-78, an analogue of the magainin antimicrobial peptides, disrupts lipid bilayer structure via positive curvature strain, Biophys. J. 84 (2003) 3052–3060.
[46] S. Yamaguchi, T. Hong, A. Waring, R.I. Lehrer, M. Hong, Solid-State NMR investigations of peptide-lipid interaction and orientation of a b-sheet antimicrobial peptide, protegrin, Biochemistry 41 (2002) 9852–9862.
[47] J.J. Buffy, M.J. McCormick, S. Wi, A. Waring, R.I. Lehrer, M. Hong, Solid-state NMR investigation of the selective perturbation of lipid bilayers by the cyclic antimicrobial peptide RTD-1, Biochemistry 43 (2004) 9800–9812.
[48] S. Yamaguchi, D. Huster, A. Waring, R.I. Lehrer, W. Kearney, B.F. Tack, M. Hong, Orientation and dynamics of an antimicrobial peptide in the lipid bilayer by solid-state NMR spectroscopy, Biophys. J. 81 (2001) 2203–2214.
[49] L. Yang, T.M. Weiss, R.I. Lehrer, H.W. Huang, Crystallization of antimicrobial pores in membranes: magainin and protegrin, Biophys. J. 79 (2000) 2002–2009.
[50] J. Butterworth, Spin echoes in solids, Proc. Phys. Soc. 86 (1965) 297–304.
[51] D.B. Fenske, H.C. Jarrell, Phosphorus-31 two-dimensional solid-state exchange NMR, Biophys. J. 59 (1991) 55–69.
[52] M. Auger, I.C. Smith, H.C. Jarrell, Slow motions in lipid bilayers. Direct detection by two-dimensional solid-state deuterium nuclear magnetic resonance, Biophys. J. 59 (1991) 31–38.
[53] F. Macquaire, M. Bloom, Membrane curvature studied using two-dimensional NMR in fluid lipid bilayers, Phys. Rev. E 51 (1995) 4735–4742.
[54] C. Dolainsky, M. Unger, M. Bloom, T.M. Bayerl, Two-dimensional exchange 2H NMR experiments of phospholipid bilayers on a spherical solid support, Phys. Rev. E 51 (1995).
[55] P.A.B. Marasinghe, J.J. Buffy, K. Schmidt-Rohr, M. Hong, Membrane curvature change induced by an antimicrobial peptide detected by ^{31}P exchange NMR, J. Phys. Chem. B 109 (2005) 22036–22044.
[56] D.G. Gorenstein. Academic Press, Orlando, FL 1984.
[57] Y. Pouny, D. Rapaport, A. Mor, P. Nicolas, Y. Shai, Interaction of antimicrobial dermaseptin and its fluorescently labeled analogs with phospholipid membranes, Biochemistry 31 (1992) 12416–12423.
[58] A. Mecke, D.-K. Lee, A. Ramamoorthy, B.G. Orr, M.M.B. Holl, Membrane thinning due to antimicrobial peptide binding: an atomic force microscopy study of MSI-78 in lipid bilayers, Biophys. J. 89 (2005) 4043–4050.
[59] A. Janshoff, D.A. Bong, C. Steinem, J.E. Johnson, M.R. Ghadiri, An animal virus-derived peptide switches membrane morphology: possible relevance to nodaviral transfection processes, Biochemistry 38 (1999) 5328–5336.
[60] K. Matsuzaki, Magainins as paradigm for the mode of action of pore forming polypeptides, Biochimica et Biophysica Acta, Reviews on Biomembranes 1376 (1998) 391–400.
[61] C. Dolainsky, P. Karakatsanis, T.M. Bayerl, Lipid domains as obstacles for lateral diffusion in supported bilayers probed at different time and length scales by two-dimensional exchange and field gradient solid state NMR, Phys. Rev. E 55 (1997) 4512–4521.
[62] J.I. Kaplan, G. Fraenkel, NMR of Chemically Exchanging Systems, Academic Press, New York, 1980.
[63] L.M. Jackman and F.A. Cotton. Academic Press, New York 1975.
[64] L. Yang, T.A. Harroun, T.M. Weiss, L. Ding, H.W. Huang, Barrel-stave model or toroidal model? A case study on mellitin pores, Biophys. J. 81 (2001) 1475–1485.
[65] K. Matsuzaki, K. Sugishita, M. Harada, N. Fujii, K. Miyajima, Interactions of an antimicrobial peptide, magainin 2, with outer and innner membranes of Gram-negative bacteria, Biochim. Biophys. Acta 1327 (1997) 119–130.
[66] K. Matsuzaki, K.-i. Sugishita, N. Ishibe, M. Ueha, S. Nakata, K. Miyajima, R.M. Epand, Relationship of membrane curvature to the formation of pores by magainin 2, Biochemistry 37 (1998) 11856–11863.
[67] F.I. Moll, T.A. Cross, Optimizing and characterizing alignment of oriented lipid bilayers containing gramicidin D, Biophys. J. 57 (1990) 351–362.
[68] S. Yamaguchi, T. Hong, A. Waring, R.I. Lehrer, M. Hong, Solid-state NMR investigations of peptide–lipid interaction and orientation of a beta-sheet, Antimicrobial Peptide, Protegrin., Biochemistry 41 (2002) 9852–9862.
[69] S. Yamaguchi, D. Huster, A. Waring, R.I. Lehrer, B.F. Tack, W. Kearney, M. Hong, Orientation and dynamics of an antimicrobial peptide in the lipid bilayer by solid-state NMR, Biophys. J. 81 (2001) 2203–2214.
[70] E. Sternin, B. Fine, M. Bloom, C.P. Tilcock, K.F. Wong, P.R. Cullis, Acyl chain orientational order in the hexagonal HII phase of phospholipid–water dispersions, Biophys. J. 54 (1988) 689–694.
[71] B. Christensen, J. Fink, R.B. Merrifield, D. Mauzerall, Channel-forming properties of cecropins and related model compounds incorporated into planar lipid membranes, Proc. Natl. Acad. Sci. U. S. A. 85 (1988) 5072–5076.
[72] J.F. Nagle, Area/lipid of bilayers from NMR, Biophys. J. 64 (1993) 1476–1481.
[73] P.L. Yeagle, A.D. Albert, K. Boesze-Battaglia, J. Young, J. Frye, Cholesterol dynamics in membranes, Biophys. J. 57 (1990) 413–424.
[74] A. Kessel, N. Ben-Tal, S. May, Interactions of cholesterol with lipid bilayers: the preferred configuration and fluctuations, Biophys. J. 81 (2001) 643–658.
[75] C.R. Mateo, A.U. Acuna, J.-C. Brochon, Liquid-crystalline phases of cholesterol/lipid bilayers as revealed by the fluorescence of trans-parinaric acid, Biophys. J. 68 (1995) 978–987.
[76] J.P. Segrest, H. De Loof, J.G. Dohlman, C.G. Brouillette, G.M. Anantharamaiah, Amphipathic helix motif: classes and properties, Proteins: Struct., Funct., and Genet. 8 (1990) 103–117.
[77] K. Matsuzaki, A. Nakamura, O. Murase, K.-i. Sugishita, N. Fujii, K. Miyajima, Modulation of Magainin 2-Lipid Bilayer Interactions by Peptide Charge, Biochemistry 36 (1997) 2104–2111.
[78] D.I. Fernandez, J.D. Gehman, F. Separovic, Membrane interactions of antimicrobial peptides from Australian frogs, Biochim. Biophys. Acta, Biomembr. (2008) in press, doi:10.1016/j.bbamem.2008.10.007.
[79] R.B. Gennis, Biomembranes: Molecular Structure and Function, Springer, New York, 1989.
[80] A.A. De Angelis, A.A. Nevzorov, S.H. Park, S.C. Howell, A.A. Mrse, S.J. Opella, High-resolution NMR spectroscopy of membrane proteins in aligned bicelles, J. Am. Chem. Soc. 126 (2004) 15340–15341.
[81] M.J. Saxton, Lateral diffusion in an archipelago. The effect of mobile obstacles, Biophys. J. 52 (1987) 989–997.
[82] J. Eisinger, J. Flores, W.P. Petersen, A milling crowd model for local and long-range obstructed lateral diffusion, Mobility of excimeric probes in the membrane of intact erythrocytes 49 (1986) 987–1001.
[83] G. Lindblom, G. Orädd, L. Rilfors, S. Morein, Regulation of lipid composition in *Acholeplasma laidlawii* and *Escherichia coli* membranes: NMR studies of lipid lateral diffusion at different growth temperatures, Biochemistry 41 (2002) 11512–11515.